Electrically activated stiffness-switching with low-melting-point conductive thermoplastics

Submitted in partial fulfillment of the requirements for

the degree of Doctor in Philosophy

in

Mechanical Engineering

Steven I. Rich

B.S., Department of Mechanical Engineering, Rice University
M.S., Department of Mechanical Engineering, Carnegie Mellon University

Carnegie Mellon University
Pittsburgh, PA

December 2018

Acknowledgments

First, I would like to thank Professor Majidi for taking me under your wing, and giving me the opportunity to finish my PhD at CMU at a time when my future was very much up in the air. Over the past three years, you have provided me with invaluable guidance on research and writing, while allowing me the freedom to guide my own research and make my own mistakes. You have pushed me to become a better researcher, and had confidence in me, even when I did not have confidence in myself. Thank you for your insight and support, and of course, for the funding.

Thank you to Professor Kowalewski, Professor Park, Professor Steif, and Professor Majidi (the committee chair) for serving on my thesis committee and sharing with me your wisdom to help me focus my research and write the best thesis I could.

Thank you to Chris and Melissa for all of your hard work to help all of the students in the department and for all of your support for student initiatives and ideas. It was really a pleasure to work with you, and I know that with you the department can only continue to improve. Also, a special thank you to Chris for helping me to navigate the challenges and bureaucracies of PhD life.

Thank you to Professor Steppan for your help with the rheometer and various aspects of rheology.

Thank you to the members of the Nanorobotics Lab and the Max Planck Institute for Intelligent Systems. Thank you to Önder, for being kankas - our trials and adventures during the first half of our PhD led us across three continents; to Guo Zhan for the guidance and advice that helped me understand what it means to do good research; to Kirstin for helping me figure out my life in a forest in Germany; to Yizhu for your infectious energy and dragging me to your eccentric hobbies and interests from bassoon ensembles to swing dance; and to Donghoon, Sukho, Xiaoguang, Hamid, Josh, Matt and all the other members of the lab for welcoming me to CMU and for helping to make my experience a positive one. Hopefully, our paths will cross again soon!

Thank you to the members of the Soft Machines (or is it Integrated Soft Materials?) Lab. Thank you to Tess - you were never too shy to provide a welcome distraction or a random snack, or to help figure out the Chinese train system; to Eric for answering my stupid questions with the utmost patience and taking what probably amounted to weeks out of your own PhD to help me finish mine. You are going to be a great professor! Thank you to Vivek for your support, philosophy, and insight on a wider range of topics than I thought humanly possible; to Sean for never hesitating to share your food, culture, knowledge, or hotel room and for putting friends way before sleep; and to Stuart, for your sense of humor, keen insight, and your temporary tattoos.

Thank you to Navid, James, Jiahe, Terri, Bugra, Chengfeng, Mo, Yun, Daniel, Hesham, and the rest of SML for creating such a fun and positive environment. I'm going to miss lab lunches at Sichuan Gourmet!

Thank you to my friends, who helped to make this experience worthwhile. Thanks to my roommates, Nathan, Rebekah, Raghav and Jay, who were always down to indulge me a late-night hangout or a cold reading of Tennessee Williams; to Celeste for all our WB chats and for everything else that helped me through my first year; to Jackson for your friendship, anime suggestions, and for letting me piggyback off your moral compass; to Katie, the house troll/Russian bear, for being there from Day 1 and for letting me bandwagon the Cubs; to Dip, for having my back and for making me question the nature of my reality; and to Rose, for your rambunctious sense of humor and for reminding me to live up to the expectations of my ancestors. Thank you to Paula, Aarudra, Phil, Satyajit, Michelle, Rei, Surya, Rahul, Nadine, Vince, Stefan, Lili, James, Will, Bowen, Cat, Samy, Sebastian and everyone else who made my time here so much more enjoyable.

Thank you to everyone who made Pittsburgh a stop (either on purpose or by accident) in the last four years: Justin, Margaret, Rachel, Josh, Ellie, Chris, Zaid, Andrew, Lizzie, Chris, Ryan, Tim, and Missy, and to everyone who let me make their homes a stop: Andrew, Kelly, Yalin, Kaye, Sean, Yizhu, Tong, Bille, Lina, Luis, Tim, Brian, Önder, Rima, Emna, Andreae, Francisco. I hope to see you all again soon!

Thank you to Nicole, Surya, Brad, Kenny, Sara, and all the folks at the GSA who helped me to become politically active and are still fighting to make the world a better place.

Thank you to Alyssa for your support over the past three years. Watching your passion and work ethic has inspired me every day, and you've helped encouraged me to do my best at everything I do.

Thank you to my parents and my sister, Carrie, without whom literally none of this would have been possible. Thank you for your love and support in so many ways!

And finally, thank you to you, reader, for bothering to read this document that I dumped 51 months of my life into. I hope you find the experience worthwhile.

This work was supported by the Samsung Global Research Outreach Program (Award #A019487), and made possible by Perstorp and their generous donation of polycaprolactone.

Abstract

As technology becomes more integrated into our daily lives, the need for machines that can safely and comfortably interact with the human body has grown. While the rigidity of traditional robotic materials, such as metals and plastics, can provide mechanical and electrical stability to these devices, it can also reduce safety and comfort when placed in contact with soft human tissue. In recent years, these issues have been addressed by incorporating compliant materials, like liquids or soft polymers, into wearable or biomedical devices. However, these materials, by virtue of their softness, cannot support the high loads required for operations like stabilization or gripping. To address this apparent trade-off between load-bearing stiffness and conformable softness, several groups have constructed stiffness-tuning devices, capable of alternating between a high-stiffness state and a low-stiffness state. Although there exist a wide variety of mechanisms by which we can achieve this switching behavior, thermally activated phase change provides the highest stiffness ratio between the soft and stiff states. In this work, use low-melting point conductive thermoplastics to create electrically activated stiffness-switching devices. When a voltage is applied across this thermoplastic, the resulting electric current causes the polymer to heat and melt. This phase change corresponds to an effective stiffness change.

In the first study, we introduce a novel stiffness switch layout that employs liquid metal as compliant electrodes oriented across the face of a conductive thermoplastic. This new layout results in an 80% decrease in required voltage, a 60% decrease in activation time, and the ability to switch the stiffness of arbitrary geometries.

In the second study, we examine the effects of the composition of a conductive thermoplastic composite on its stiffness-switching properties, and use these findings can help guide the design of stiffness-switching composites for a three soft robotic applications.

Contents

List of Figures

1

Introduction[1]

Recent work into soft robotics[1,2,3,4,5] and flexible electronics has sought to improve the biocompatibility and versatility of conventional robots in unstructured environments. Often, these devices take inspiration from biology, mimicking the elasticity of skin to improve the impedance matching of human-machine interfaces, or imitating the softness and flexibility of organisms like the octopus (Figure 1.1) to adapt to real-world environments and thereby create novel robotic functionalities. Electric materials with compliance comparable to this biological tissue are particularly important for human-machine interaction[6,7], wearable computing[8,9], health monitoring[10,11] and physically assistive robotics[12,13], because they are intrinsically safe and comfortable.

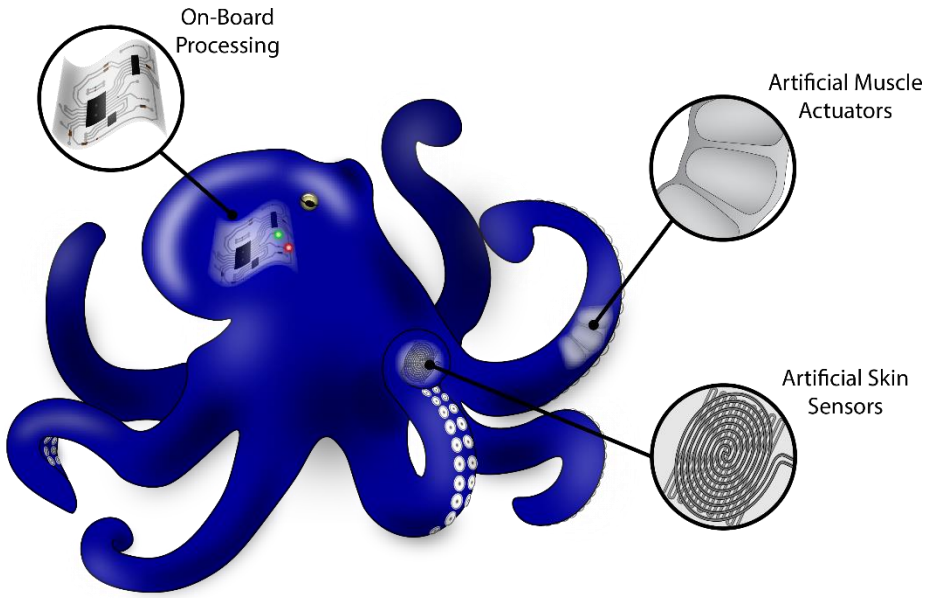

Figure 1.1: Artist's conception of a fully soft octopus robot, that imagines ways in which actuation, sensing, and processing could be implemented in an advanced soft robot[4].

[1] To the reader: if you would like an easier-to-read version of this document that does not have to comply with ProQuest's formatting restrictions, please contact me.

As the field of soft robotics gradually moves toward the mainstream of tech, it brings a diverse palette of materials and material properties to the engineering toolbox[14]. Elasticity itself has become a critical feature of any device expected to interact with humans or adapt to its environment, and many groups have worked to recreate conventional electronic systems within this new soft paradigm[15,16,17]. While many applications that arise from this fresh mindset take advantage of the comfort and adaptability of soft materials, they can often require the strength and load-bearing capacity of conventional stiff materials as well[18,19].

Many biological organisms have faced a similar paradox: How can a soft-bodied octopus find shelter by squeezing into a tiny crevice, yet still exert enough force to catch fish with its tentacles? How can our muscles gently stretch without tearing, yet apply large forces to lift a heavy barbell? How can a sea cucumber with no skeleton navigate its environment, yet protect itself from predators?

Ultimately, evolution has converged on several different types of biological tissues — muscular hydrostats[20], skeletal muscle[21], and catch connective tissue[22], respectively — that allow these organisms to reversibly change the stiffness of their body parts. Finding inspiration from these organisms, we can design **stiffness-tuning** devices that can take advantage of the beneficial properties of both soft and stiff materials.

These materials may one day enable technologies like conformable grippers capable of handling heavy loads, powerful industrial robots that work safely alongside humans, soft robots that navigate and manipulate their environment as quickly and effectively as animals, surgical tools that minimize the amount of trauma inflicted on the body, prosthetics that mimic and even improve their human counterparts, and wearable devices that provide a perfect fit to their user.

There have been a wide variety of approaches to address the question of stiffness tuning, each with its own set of benefits and challenges. These methods will be discussed in detail in the following section.

1.1 Types of Variable Stiffness Devices

The two fundamental factors when determining the potential applications of a stiffness-switching material[2] are 1) the directionality of the transition (i.e. soft-to-stiff or stiff-to-soft) and 2) the speed of the transition. The directionality of a stiffness switch determines which rigidity state (stiff or soft) is its default and which state requires the continuous input of energy. As no work has demonstrated stability over multiple stiffness states, the passive state should correspond to the state in which the majority of the lifetime of the device is spent. The speed of the stiffness transition effectively determines whether the device can be used in dynamic or quasi-static applications, and therefore refers to the speed of both stiffening and softening for a given device.

The combination of these properties yields four theoretical categories of stiffness-switching material:

I. **Dynamic stiffening** requires a material to quickly change from a passive soft state to an active stiff state and back, allowing for an artificial muscle actuator to instantaneously apply a force. This feature is analogous to skeletal muscle[21], which

[2] We draw the distinction between **stiffness-tuning device**, those that can tune their stiffness along a continuum of states, and **stiffness-switching device** or **stiffness switches**, those that can alternate between a high-stiffness state and a low-stiffness state. Although many stiffness-switching devices in the literature refer to themselves as stiffness tuning (including one work by this author), we believe this nomenclature to be misleading. Examples of true artificial stiffness-tuning materials are rare; therefore, the following discussion will focus on stiffness-switching materials.

makes these devices especially useful in robotic systems that may require load bearing. In particular, they can be used in domains like soft locomotion, assistive devices, gripping and manufacturing, and potentially in soft robotic defense. To achieve this rapid change in state, these devices must be based on quick-responding media, such as pressure and electricity.

II. **Quasi-static stiffening** requires a material to change from a passive soft state to an active stiff state and back, without any speed or bandwidth constraints. In biology, this can be found in the catch connective tissue of sea cucumbers[22], which enables both locomotion and rapid defense response, or in the erectile tissue of mammals. Because of this slower actuation speed, quasi-static stiffening is best suited for responding to environmental stimuli.

III. **Dynamic softening** requires a material to quickly change from a passive stiff state to an active soft state and back. In robotic systems, this feature may be applicable to situations where damping or energy absorbance is desired, for instance, when improving the safety of potentially harmful interactions between robots and humans.

IV. **Quasi-static softening** requires a material to change from a passive stiff state to an active soft state, without any speed or bandwidth constraints. This feature is particularly useful in shape adaptation, which may be applicable in wearable devices or certain robotic manipulation schemes. These devices are typically based on materials that can create a large change in stiffness, such as phase-change materials.

Another class of stiffness-change materials include those with non-reversible transitions.

Often these materials are responsive to changes in the environment, and can be used to create smart responses to certain stimuli[23]; however, because their stiffness cannot be fully controlled, they will not be discussed further in this thesis.

1.1.1 Dynamic Stiffening

In order to achieve high bandwidth, high switching ratio[3] actuation, dynamic stiffening devices employ mechanisms that are capable of rapidly transmitting force based on electricity, fluid pressure, and magnetic field.

Pneumatics and Hydraulics Pneumatics and hydraulics are types of pressure-based stiffness-tuning devices that are commonly used in soft robotics. Similar to muscular hydrostats found in the animal kingdom, these actuators control bending in soft continua by changing the pressure in sealed cavities[20]. However, when this motion is countered by other actuators working in opposition (e.g. muscles[20], wire tendons[24,25,26,27], other pressure-based actuators[28,29]), it is possible to achieve a rapid increase in overall stiffness. With these devices, stiffness can be tuned, rather than simply switched between a high- and a low-stiffness states; however, this change is typically modest, and achieving it typically requires a pump[18]. Incompressible fluids, like oil and water, enable pressure-based stiffness change without the use of a pump[30,31]; however, these methods are not as versatile as standard pneumatics in terms of layout. Pressure-based stiffness-tuning devices are often useful when coupled with other actuation schemes to help control the shape or stiffness of continuum robotic limbs[29] for use in surgical[25,26],

[3] Switching ratio refers to the ratio between the maximum stiffness and the minimum stiffness achieved by the device.

prosthetic[24], or manipulation[28,32,27] applications.

Jamming Materials Although jamming-based devices can achieve a rapid stiffness increase by changing their internal pressure, the mechanism of stiffness change is distinct from that of pneumatic stiffness-tuning devices. When a vacuum is applied to a soft cavity filled with particles[33,34,35,36,37,38,39,40] or sheets [41,42,43,44,45,46], atmospheric pressure compresses these components together, causing an increase in frictional force that manifests as an increase in the bulk stiffness of the device. This change in stiffness can be very large and very rapid, but is dependent on the performance of the pump. Particle jamming has been widely used to create universal grippers capable of rapidly from changing a low-stiffness state, in which they conform to an object, to a high-stiffness state, in which they can support the object's weight[33]. Both particle and sheet (also known as layer) jamming are also useful in **shape-locking**[4] applications, allowing wearable devices to give support or apply force to a human subject[43,34,41,44], providing rapid haptic feedback to soft user interfaces[35,45,37], and enhancing the controllability and stability of soft robotic actuators[36,38], often in surgical applications[46,39,40].

Electrostatics Electrostatic stiffness switches also achieve a rapid increase in stiffness by changing the frictional force between thin sheets. Instead of applying a normal force to push these sheets together through pressure, as jamming-based stiffness tuning devices do, these devices apply a normal force through electrostatic attraction. When the opposite voltage on two adjacent sheets is high enough, they become attracted to one another. If a high-friction dielectric material lies between these electrodes, a high frictional force will arise when they come in

[4] **shape-locking**: the ability of a stiffness-tuning device to freeze a certain configuration by increasing the stiffness while in a deformed state

contact. These actuators use high voltages (> 200 V) to generate a strong normal force; however, they devices lightweight and low-power, and generate dramatic changes in stiffness at a high frequency[47,48,49]. This makes them particularly suitable to high-speed human-centric robotic applications, including exoskeleton actuation[47], robotic gripping[50], and wearable haptics[49]. By stacking multiple dielectric elastomer actuator (DEA) electrodes, electrostatic stiffness switches can show a dramatic increase in bending stiffness, similar to vacuum-based layer jamming, that enables applications such as soft robotic gripping[51].

1.1.2 Quasi-static Stiffening

Reversible quasi-static stiffness switching is fairly uncommon among stiffness change modalities. The most common method of achieving this mode of stiffness change is through shape-memory alloys (SMAs).

Shape-Memory Alloys SMAs are alloys that are capable of achieving a change in stiffness by reversibly transitioning between solid crystalline phases. Above a certain temperature, these materials change from martensite to austenite, which is associated with a modest increase in stiffness and often a deflection. As they cool, they transition back to martensite, and regain their original stiffness and configuration. Although these materials can undergo a relatively rapid change in stiffness, they are fundamentally constrained by the speed of heat transfer during their de-stiffening process. Thus, although they have been popular for soft robot applications[52,53,54], their use has been limited in highly dynamic systems. Additionally, since these changes in stiffness are typically coupled with a movement, SMAs used in stiffness-tuning devices are often arranged in antagonistic architectures with other elements[55,56,57,58]. As a result, they are

infrequently used, but have been implemented in vibration control[59,60] and surgical robotics[61,58].

1.1.3 Dynamic Softening

Dynamic softening is currently very rare, and can be achieved by modifying a dynamic stiffening scheme to reverse the passive and active stiffness states. For instance, to achieve a robotic manipulator that can instantaneously soften when in the proximity of humans, Stilli et al. propose a highly-pressurized pneumatic robotic link that can abruptly release pressure[62].

1.1.4 Quasi-static Softening

The most common form of quasi-static softening employs materials that undergo a temperature-dependent change in mechanical properties at a relatively low temperature, including low-melting-point alloys (LMPAs) and metals, low-melting-point thermoplastics, and shape-memory polymers (SMPs). Some chemoresponsive materials also show quasi-static softening.

Chemoresponsive Materials A common type of chemoresponsive stiffness-tuning materials are polymer nanocomposites that can reversibly decrease their stiffness when exposed to certain chemicals. The interactions between the nanofiber networks embedded in these polymers change with the presence of various substances, including deionized water, ionized water, or high pH fluid, causing a change in the stiffness of the bulk material[63,64,65,66]. Although the switching ratio of this response is high, the response time is very slow, severely limiting the applicability

of these materials. We also note that it is possible to view many of these materials as quasi-static stiffening, depending on whether the presence or absence of the activating substances is considered the "default" state. One alternative method by Ren et al. exploited the soluble crosslinks of a polyvinyl formal sponge to control the stiffness of a tube with a water vapor pump[62]. They incorporated this material into a surgical actuator and a splint.

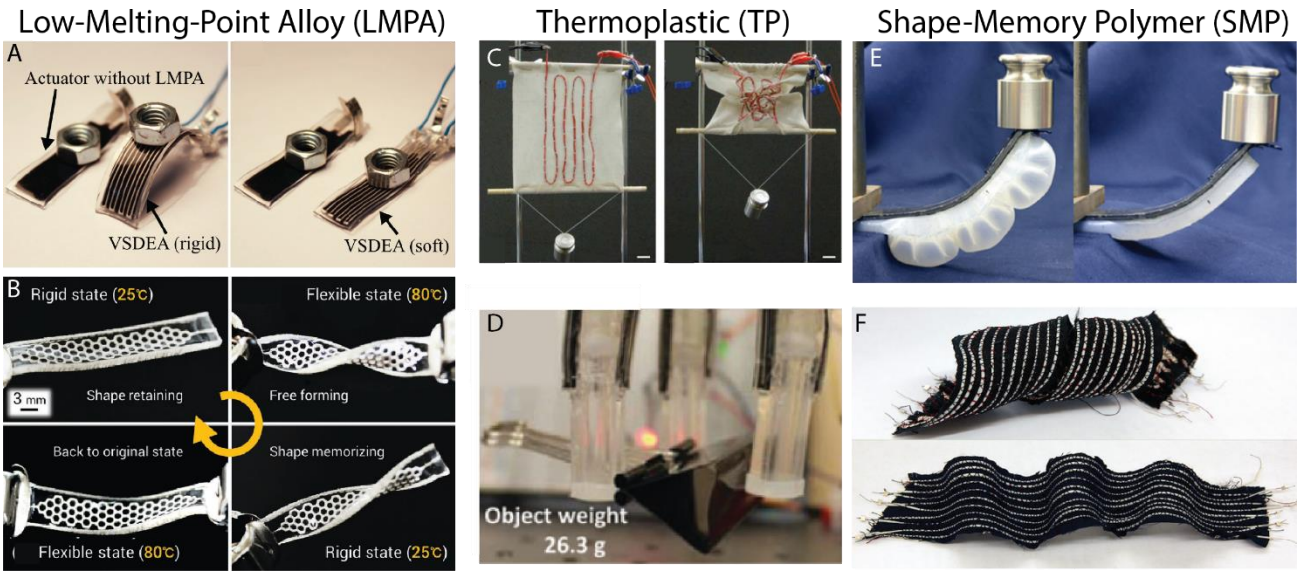

Figure 1.2: Overview of thermally activated stiffness-switching technologies, including low-melting-point alloys (LMPAs): (A) ©2015 IEEE. Reprinted with permission from [67]; (B) ©2018 John Wiley and Sons. Reused with permission from [68]; low-melting-point polymers: (C) ©2016 IEEE. Reprinted with permission from [69]; (D) ©2017 Mary Ann Libert, Inc. [70]; and shape-memory polymers (SMPs): (E) ©2017 IEEE. Reprinted with permission from [71]; (F) ©2014 IEEE. Reprinted with permission from [72]

Low-Melting-Point Alloys and Metals LMPAs, such as Field's metal and Wood's metal, are alloys that can be melted at relatively low temperatures (<80 ◦C). Embedded in an elastomer or gel casing at room temperature, the solid LMPA imparts a high metallic stiffness to the overall structure. When the system is heated above the melting point of the LMPA, the overall stiffness becomes dominated by that of the softer elastomer, until the liquid metal cools and resolidifies

(Figure 1.2 A-B). Because of the high stiffness of these metals and the low stiffness of the casing, many of these devices have very high switching ratios[73,74,68], though the high heat of fusion can sometimes lead to long activation times[74,75]. If the casing is sufficiently elastic, these devices can also demonstrate a shape-memory effect[76,68]. In many cases, LMPA-based stiffness switches are actuated using external heaters; however, since, as metals, these materials are electrically conductive, a voltage can be applied across a length of an LMPA wire, resulting in Joule heating. If the applied power is sufficient, this heating can induce melting in the alloy, yielding an electrically actuated stiffness change[74,77,67,78,75,79].

This large and reversible change in stiffness makes these stiffness switches ideal candidates for strong remoldable devices such as inductors[78] or splints[73] that can conform to irregular geometries. LMPA-based stiffness switches can also be used in soft robotic systems, creating customizable configurations by softening LMPA located at critical joints[75,73,80], improving dexterity and stability of catheters through selective stiffness control[81], or strengthening the load-bearing capacity of grippers without sacrificing flexibility[67,79,82,80]. On small scales, low-melting-point metals can be even used without a casing, for manipulation and adhesion applications, thanks to the passivating oxide layer that natively coats gallium[83].

Low-Melting-Point Polymers Like LMPAs, low-melting-point thermoplastics transition to polymer melts after being heated to relatively low temperatures (<80 ◦C). Stiff at low temperatures, these materials can be embedded in soft elastomer casing, forming a stiffness switch with high overall stiffness. When the system is heated, the polymer melts, and the rigidity of the overall structure becomes dominated by that of the soft elastomer, until the polymer cools and resolidifies (Figure 1.2 C-D). Because polymeric materials are typically less rigid than

metals, thermoplastic-based stiffness switches often have a lower switching ratio than LMPA-based switches[19]. However, when compared with LMPAs, these materials are low-cost, readily available, and easily printable[84] or patternable[85,86,87] with a blade or a laser cutter. They are also lightweight, which is both convenient for wearable devices such as moldable orthotics[84,85] and also dramatically reduces the energy input required to melt the material, leading to faster activation and deactivation times. Low-melting-point thermoplastics stiffness-switching has been employed in soft robotic systems to control robotic joints and ligaments[85,70,88,69], and maneuver endoscopes and catheters[89,90].

Although many of these systems employ external heaters, it is also possible to use conductive thermoplastic to induce resistive heating directly in the stiffness-switching element[85,87,70,86,84,91]. These designs can simplify the layout of the device and reduce energy requirements by minimizing the heat transferred to auxiliary components.

Shape-Memory Polymers SMPs are typically thermosets with a low glass transition temperature (<80 °C), and can also be useful in stiffness switches. When heated above their glass transition temperature, these materials can soften significantly, returning to their rigid state when they are cooled (Figure 1.2 E-F). Their maximum stiffness generally lies between LMPAs and low-melting-point thermoplastics, while their minimum stiffness is higher than both, resulting in an intermediate switching ratio[19]. The transition temperature for these materials is often very low (<50 °C), enabling simple switching. Although they are not as remoldable as thermoplastic polymers, SMPs can undergo bending and mild extension[92,93,94,74], and can serve as active hinges[95,96,97] or work to hold the shape of soft actuators and grippers under load[71,98,96,99,72,100,97,101]. Like conductive thermoplastics and LMPAs, these materials may be

heated either externally or directly, using resistive heating to activate conductive SMPs[71].

1.2 Contribution

In this thesis, we continue the development of stiffness-switching materials based on low-melting-point conductive thermoplastics (cTP), seeking to address the problems with the current state-of-the-art in quasi-static softening, such as high voltages, low stretchability, and stringent geometric constraints. We present a novel materials architecture to improve the accessibility and versatility of stiffness-switching devices, and develop a framework to aid in the formulation of new stiffness composites for a variety of soft-robotic and wearable applications.

Novel Materials Architecture: We develop a new materials layout that improves performance and introduces novel functionality to stiffness switches. By incorporating a non-traditional electrode material (liquid-metal alloys) in a through-thickness orientation, we dramatically reduce the activation time and voltage, and enable the activation of sheets of an arbitrary geometry.

Composition Studies: We study the effects of the composition of a cTP-based composite on a potential stiffness switch. We propose these findings to guide the development of future cTP-based devices for use in diverse applications.

This thesis is organized into four chapters. In the current chapter (Chapter 1), we provide an overview of stiffness-switching and describe the different classes of stiffness-switching applications. We then detail a novel materials architecture (Chapter 2), and describe how the

behavior of a stiffness-switching device can be controlled by changing its composition (Chapter 3). Finally, we conclude with a discussion of future work and an outlook for stiffness-switching devices.

2

Liquid Metal Electrodes for Low-Voltage Stiffness-Switching of Conductive Thermoplastics[5]

2.1 Background

For thousands of years, humans have incorporated rigid components into their clothing and accessories for protection[102], medical support[103], aesthetics[104], and load-bearing[105]. When the fit between body and garment is not perfectly calibrated, the mismatch in stiffness between these materials and human tissues can cause discomfort or injury. Recent attempts to improve this interface have focused on technologies such as 3D printing to customize the shape of these garments[106]; however, these bespoke components cannot adapt to the changes in an individual's body that can occur over months or years. Stiffness-switching composites provide a convenient method for rapidly adapting the fit of rigid garments on-the-go. Although pneumatics[24], jamming[43,34,42], and dielectric elastomer actuators[51] have been used effectively for stiffness switching or stiffness tuning, stiffness-switching wearables are best served by **quasi-static softening** materials[19].

Thermally activated stiffness switching composites, conversely, are stiff in the passive state, and can enable reliable, high-switching-ratio stiffness switches that are not confined to specific geometries and layouts[89,68]. Although attempts to improve the fit of such rigid garments using heat-activated stiffness switching extend back millennia[107], recent work has focused on using

[5] This work was completed in collaboration with Dr. Sung-Hwan Jang, Professor Yong-Lae Park, and Professor Carmel Majidi. [85]

electrically conductive materials, such as low-melting-point alloys (LMPAs) or low-melting-point conductive polymers, to achieve electrical actuation, minimizing thermal losses and auxiliary equipment requirements. Historically, LMPAs have been a common choice for stiffness-switching elements[68,73,74,77]; however, conductive polymers have gained popularity in recent years thanks to their light weight, low cost, and simple processing methods. Conductive polymers have previously been employed as resistive strain sensors[108] or electrical interconnects in additive manufacturing[109], but recent work has revealed their potential as electrically activated stiffness switches[86,70,71] (Table 2.1). Although these devices are exciting steps toward adaptable wearables, they can be hindered by long activation times, high activation voltages, and limited scalability and structural versatility. At present, there remains to be an electrically powered method for reversible stiffness switching that exhibits <5s, <20V actuation in a size-scalable architecture that allows for integration into a wide variety of systems.

In this chapter, I introduce a stiffness-switching material architecture that changes between a high-stiffness state and a low-stiffness state in response to moderate electrical voltage achievable with a standard battery or power supply. Furthermore, I demonstrate its feasibility in both tensile and flexural applications via an active tendon in an underactuated robotic finger model and a moldable splint.

Author (Year)	Activation Time (s)	Voltage (V)	Stiffness Ratio	Material
Rich et al. (2017)[85] (*This Work*)	2-40	5-20	15	cTP
Le et al. (2017)[89]	30	External Heating	55	TP
Buckner et al. (2017)[71]	10	Variable	37	cSMP
Yang et al. (2017)[95]	40	External Heating	10	SMP
Tonazzini et al. (2016)[73]	29	External Heating	700	LMPA
Van Meerbeek et al. (2016)[76]	Not Reported	External Heating	18	LMPA
Zheng et al. (2015)[75]	60-160	4-5	Not Reported	LMPA
Shan et al. (2015)[86]	6	100	25	cTP
Balasubramanian et al. (2014)[98]	2	External Heating	76	SMP
Schubert et al. (2013)[77]	1	Not Reported	27	LMPA
Shan et al. (2013)[74]	130	0.6	9033	LMPA, SMP
McKnight et al. (2010)[93]	>60	Not Reported	77	SMP

Table 2.1: Comparison of phase change stiffness-switching technologies. Acronyms: **cTP** - conductive thermoplastic, **TP** - thermoplastic, **cSMP** - conductive shape memory polymer, **SMP** - shape memory polymer, **LMPA** - low-melting-point-alloy.

2.2 Stiffness Switch Design and Fabrication

The stiffness switch is composed of a conductive thermoplastic (cTP) stiffness-switching element that is coated on opposite faces by a thin layer of liquid metal alloy, and surrounded by a silicone elastomer casing (Figure 2.1). Because the cTP is significantly stiffer than the silicone elastomer, the overall stiffness of the device is high when the cTP is unactivated. When a voltage is applied to the liquid metal electrodes, current flows through the thickness of the composite, inducing resistive heating that causes the thermoplastic to melt within several seconds. This phase change dramatically reduces the effective stiffness of the cTP, causing the overall stiffness to converge to the lower stiffness of the elastomer casing. When the voltage is removed, the cTP gradually resolidifies, once again imparting its high stiffness to the device.

By orienting the electrodes across the thickness of the device, the resistance of the cTP circuit is reduced by several orders of magnitude. This means that the activation voltage can be dramatically reduced, without affecting the heating rate of the composite. Conversely, very high

heating rates can be achieved when the voltage is not reduced. Furthermore, because current flows linearly between the two electrodes, this through-thickness arrangement means the actuation area is dependent on the shape of the electrodes, contrasting with the straight-line actuation area formed between two electrodes in a length-wise configuration.

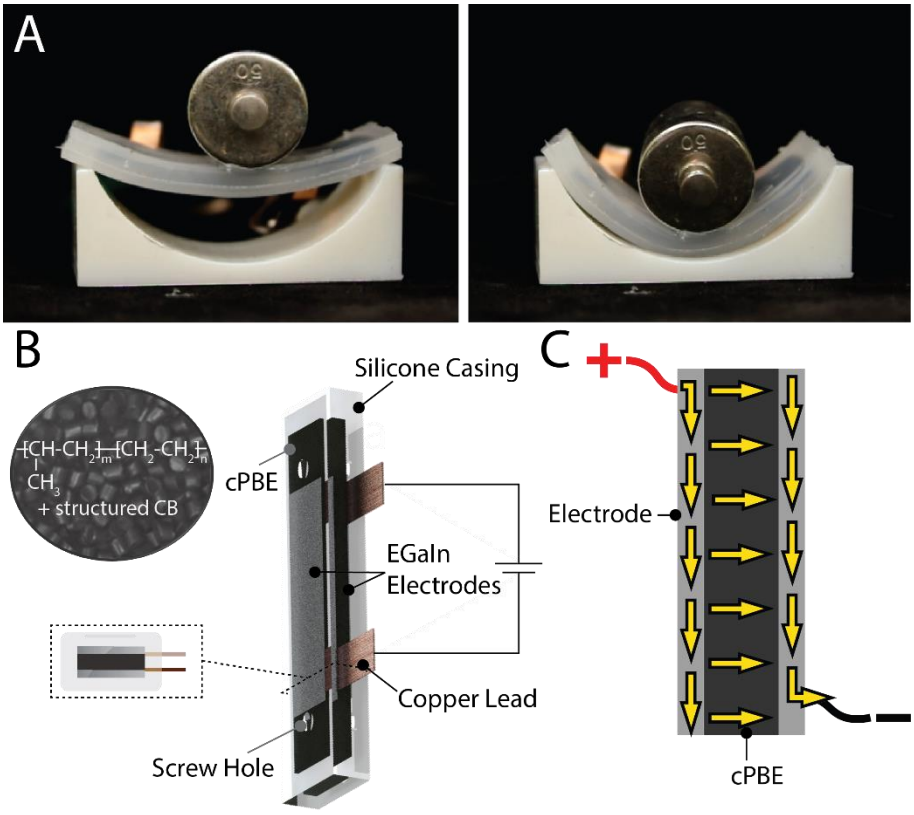

Figure 2.1: Overview of layout and actuation of a stiffness switch based on conductive polypropylene-based elastomer (cPBE). (A) The switch in the stiff state (left) and the soft state (right) after being actuated with 5 V, (B) The layout of the switch showing the composition, the through-thickness arrangement of the eutectic gallium-indium (EGaIn) electrodes, and the interface between the copper and the EGaIn, (C) The direction of current moving first along the highly conductive EGaIn electrodes, then through the thickness of an actuated cTP layer.

For this study, we use a conductive polypropylene-based thermoplastic elastomer (cPBE), composed of a copolymer of polypropylene and polyethylene, filled with a percolating dispersion of structured carbon black (weight-composition: 51/9/40%). The stiffness tuning

elements were formed by compressing pellets of this polymer (THEMIX Plastics Inc.) to a thickness of 1.1 mm using a hydraulic heat press (Model C 3912, Carver) at a temperature of 160 °C, and cutting the resulting sheets into 5 cm × 1 cm using a 30 W CO_2 laser(VLS 3.50, Universal Laser Systems). Copper strips were embedded into the surface of these strips using the heat press at 160 °C to provide a stable mechanical connection to the voltage source. Eutectic gallium indium (EGaIn, Rotometals) was deposited on both faces of the strips using a spray gun (40 psi, with argon gas as a carrier), coating the copper strips, but avoiding the portions of the strip that would form the mechanical interface with the testing set-up. The strips were symmetrically embedded in a 3 mm casing of silicone rubber (E = 0.4 ± 0.03 MPa; Ecoflex 00-30, Smooth-On): a lower layer of silicone was cured in a mold printed from a 3D printer (Objet 24, Stratsys), the EGaIn-painted cTP was aligned with the embedding layer, and a secondary mold was screwed onto the base mold to allow another layer of silicone to be poured over top. All samples were degassed and cured in an oven at 80 °C.

In order to activate the cTPs, alligator clips were attached to the copper leads, and a voltage was applied using a DC power supply (Model Digi 360, Electro Industries). An IR camera (C2, FLIR) was used to ensure the composite heated equally across its surface, allowing us to determine when the external temperature of the

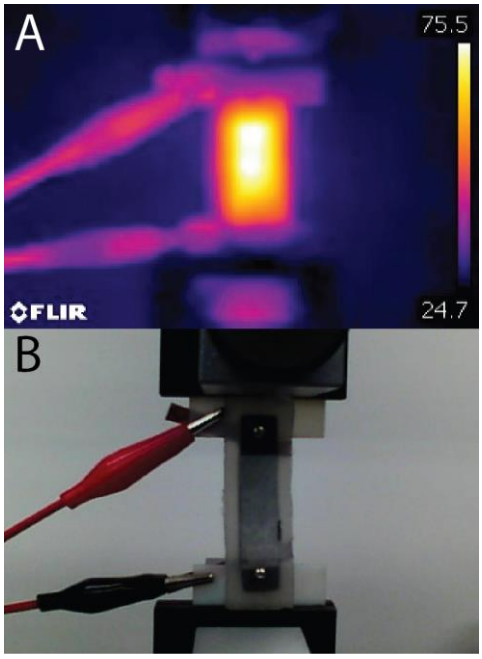

Figure 2.2: Through-thickness stiffness switch undergoing activation: (A) IR photograph taken from 10 cm (B) visible light photograph, taken simultaneously. There is even heating across the composite.

switch had reached 75 ℃ (Figure 2.2). When the IR camera read a temperature of 75 ℃, the actual temperature of the stiffness-switching element was likely higher than the measured value, because the silicone rubber acted as a thermal insulator. Since any temperature above 72.9 ℃ was sufficient for melting, we could ensure the cPBE was in the activated state. All measurements in the activated state were made at 75 ◦C as measured by the IR camera, while measurements in the unactivated state were made at room temperature. Unless otherwise specified, all activation voltages were 5 V.

2.3 Thermal Characterization and Modeling

To determine the activation mechanism and energy requirements for cPBE actuation, differential scanning calorimetry (DSC) was performed on an 8.8 mg sample (DSC Q20, TA Instruments). Temperature was cycled between -80 ◦C and 150 ◦C, at a rate of 10 ◦C min−1 for four cycles. The dynamic mechanical behavior[6] of cPBE was evaluated using the tension mode on a dynamic mechanical analyzer (Model 2980, TA Instruments). The samples were prepared with a dimension of 15.0 mm × 5.0 mm × 0.5 mm. The storage modulus was determined by straining the sample at a frequency of 1.0 Hz and amplitude of 50 μm. The temperature was increased from −40 °C to 80 °C at a rate of 3 °C min−1.

The cPBE composite shows a glass transition below −60 °C, a melting peak at 72.9 °C ± 0.07 °C, and a crystallization peak at 59.8 °C ± 0.07 °C (Figure). This suggests that electrically induced cPBE softening is caused by a solid-liquid phase transition rather than a glass transition or Vicat softening, as previously claimed for a cPBE composition [86]. Such results are consistent with measurements obtained using dynamical mechanical analysis (DMA), which is

[6] DMA tests were performed by Dr. Sung-Hwan Jang (Plymouth University).

shown in the inset of Figure 2.3. As expected, we observe a significant drop in storage modulus and a peak in damping factor as the temperature exceeds 75 °C. Above this temperature, the

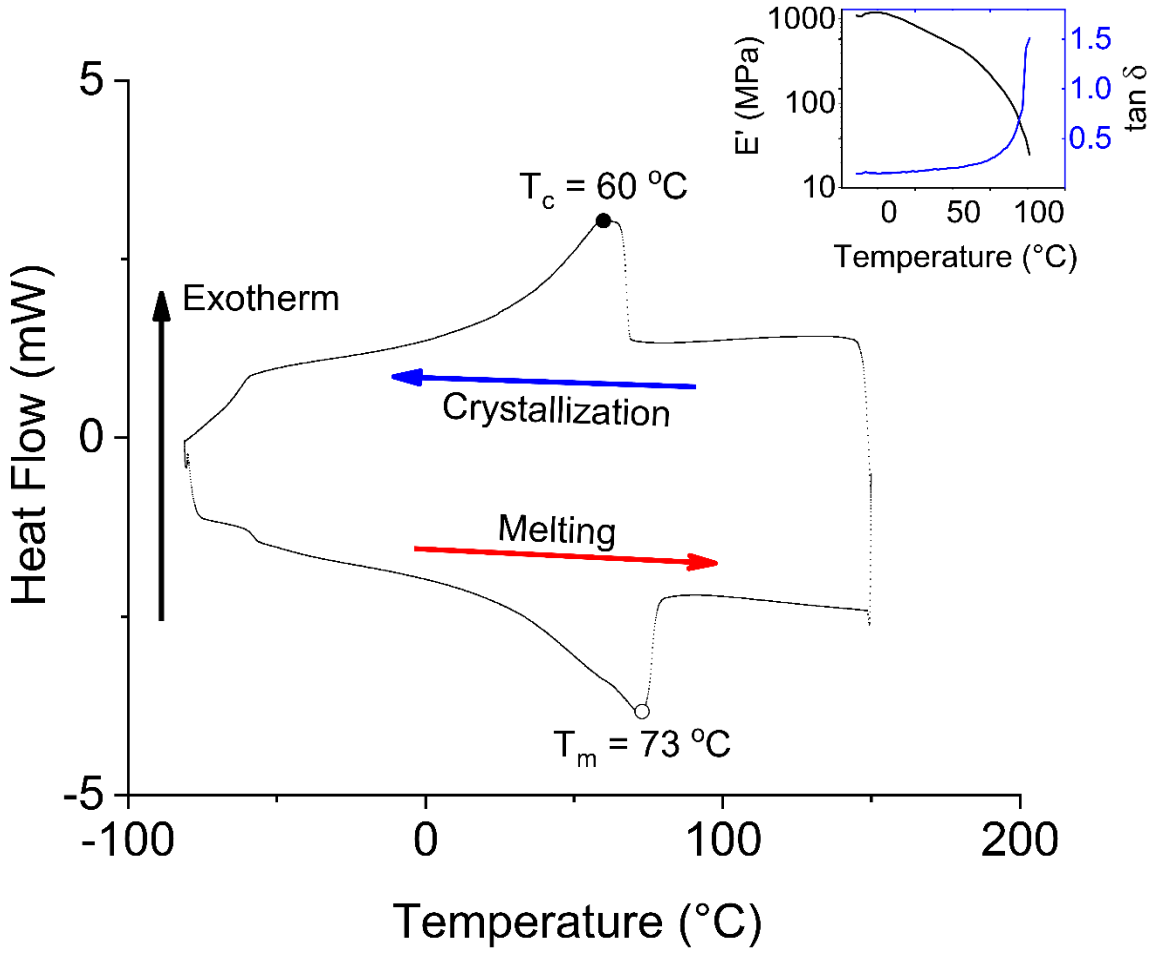

Figure 2.3: Differential scanning calorimetry plot of cTP between -80 °C and 150 °C. This plot shows the second heating cycle with the exothermic direction oriented upward. The first cycle shows some abnormalities due to thermal stresses, but in cycles 2-4, the behavior converges. The peak at 72.9 °C indicates the melting temperature (Tm), while the peak at 60 °C represents the crystallization temperature (Tc). The kink between -80 °C and -50 °C represents the glass transition temperature; however, this value cannot be determined without examining the heat flow at lower temperatures. The inset shows DMA data, which corroborate the softening temperature found in the DSC data.

storage modulus is approximately one order of magnitude smaller than that measured at room temperature. Although the addition of fillers such as carbon black may slightly change the thermal properties of the host matrix material, the values found in the DSC and DMA

measurements resemble those of the unfilled propylene-ethylene copolymer[110]. We note that the DSC plot shows a melting peak offset 13 ◦C higher than crystallization peak, revealing some thermal hysteresis in the material. The lower crystallization temperature indicates a potential delay in the restiffening response when integrated in the device.

Based on the thermal properties of the cPBE gathered from the DSC tests and fundamental heat transfer equations, we next sought to determine the required energy input to achieve activation, when the composite is incorporated in a stiffness-switching device. We assume that under applied voltage, the cTP functions as an ideal Joule heater, transforming electrical energy to heat in order to reach the activation temperature, T_a. The effect of this heating can be seen in the infrared photograph in Figure 2.2. This process can be described using conservation of energy:

$$E_{req} = E_{st} + E_o \tag{2.1}$$

where E_{req} is the required energy input, E_{st} is the energy stored within the switch, and E_o is the energy released. To find the E_{req} required to induce phase change, we examine the components of the right side of the equation.

The stored energy, E_{st}, is composed of the change in enthalpy of the cTP required to induce melting from room temperature (ΔH_a) and the heat stored in the surrounding silicone matrix (ΔH_{sil}). Because heat is dissipated from the surface of the switch by convection and radiation (conduction is neglected, since the switch is attached to the test set-up at the unactivated screw holes), the energy released, E_o, can be expressed as the sum of the heat lost to convection (ΔH_{conv}) and the heat lost to radiation (ΔH_{rad}). Thus, we see

$$E_{req} = \Delta H_a + \Delta H_{sil} + \Delta H_{conv} + \Delta H_{rad} \tag{2.2}$$

We can find ΔH_a by integrating the area beneath the melting peak of the DSC plot (located in the lower half of the heating loop in Figure 2.3) and dividing by the heating/cooling rate (10 K min^{-1}) and the mass of the sample (8.8 mg). This yields a heat of 112.8 J g^{-1}. Given a cPBE mass of 0.72 g in each stiffness switch, we find ΔH_a = 81.2 J.

ΔH_{sil} can be expressed by the equation

$$\Delta H_{sil} = \rho V C_p (T_f - T_\infty) \tag{2.3}$$

where ρ is the density of the silicone (1064 kg m^{-3}), V is the volume (3 mm × 50 mm × 13 mm = 1.95 × 10^{-6} m^3), C_p is its specific heat capacity (1050 J kg^{-1} K^{-1}), T_f is the max temperature when activation occurs (75 ◦C), and T_∞ is the starting (i.e. ambient) temperature (25 ◦C). Using these figures, we find, ΔH_{sil} = 108.9 J.

We note that the magnitude of the losses due to convection and radiation is highly dependent on both activation time and surface temperature, which means that the applied voltage can have a significant impact on the amount of energy dissipated. We select 5 V as an example and solve for ΔH_{conv} and ΔH_{rad}.

The heat lost to convection is given by

$$\Delta H_{conv} = \int_0^{t_a} q dt = \int_0^{t_a} hA(T_s - T_\infty) dt \tag{2.4}$$

where t_a is the activation time, given by the point where the stiffness drops by 90% of its total drop, q is the heat transfer rate, h is the convective heat transfer coefficient ($\sim$ 15.5 Wm^{-2} K^{-1}), A is the convective area of the switch (2 × 50 mm × 13 mm = 1300 mm^2), T_s is the surface temperature of the switch as a function of time, and T_∞ is the ambient temperature (25 °C). With h and A constant, we can calculate $\int_0^{t_a} (T_s - T_\infty) dt$ by taking the area between the measured temperature and the ambient temperature on the temperature-time plot created from the IR camera measurements (Figure 2.4). Since the camera measures surface temperature, the

temperature on this plot is an accurate measure of T_s. From the integral's value of 3220 K s, we find ΔH_{conv} = 64.9 J.

Finally, we calculate the heat lost to radiation, given by

$$\Delta H_{rad} = \int_0^{t_a} q dt = \int_0^{t_a} \varepsilon \sigma T_s^4 dt \quad (2.5)$$

where ε is the emissivity (~0.95), and σ is the Stefan-Boltzmann constant (5.67×10^{-8} $Wm^{-2}K^{-4}$). As before, with ε, σ, and A constant, we can calculate the integral $\int_0^{t_a} T_s^4 dt$ from the IR camera plot (Figure 2.4). This value is 8.20×10^{11} K^4s, from which we find ΔH_{rad} = 57.4 J.

Plugging these values back into our energy balance equation, we find the energy required to activate a cTP element:

$$E_{req} = 81.2 \text{ J} + 108.9 \text{ J} + 64.9 \text{ J} + 57.4 \text{ J} = 288.1 \text{ J} \quad (2.6)$$

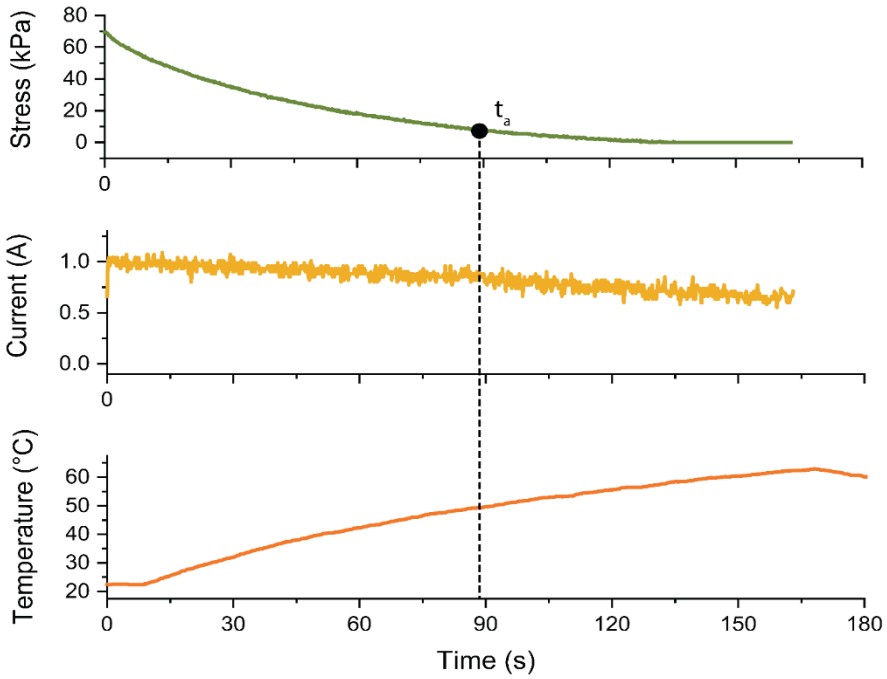

Figure 2.4: Plot of stress relaxation, current, and temperature over time as voltage is applied to a prestrained stiffness switch. T_a is indicated when stress has declined 90% from the total drop. Current declines slightly over time, indicating increased resistance. Temperature increases after several seconds, indicating that there is some delay beween the heat measured by the camera at the surface and the heat generated by the cTP.

The value of each of these enthalpies and the total energy required is shown in Table 2.2.

We can then calculate, E_i, the expression for electrical energy input, given by the integral of the power input - or the integral of the current input multiplied by the scalar voltage (Figure 2.4), yielding

$$E_i = \int_0^{t_a} P dt = \int_0^{t_a} VI dt = \int_0^{t_a} \frac{V^2}{R} dt \qquad (2.7)$$

where V is the applied voltage, I is the current through the cTP, and R is the resistance of the cTP. The right side of Equation 2.7 represents the scaling law that shows that for a prescribed energy input, E_i, minimizing the cTP resistance R can permit low-voltage activation, achievable with a 9 V battery. For these calculations, V is held constant (5 V), but I changes as a function of time because the resistance of the cTP changes as it heats up. $\int_0^{t_a} I dt$ can be calculated from the current-time plot in Figure 2.4, yielding 75.7 A s, from which we calculate E_i = 409.4 J. These input energies are shown in Table 2.2.

We would expect these input energies to match the required heat for each voltage; however,

Voltage	Energy Released					Energy Input
(V)	ΔH_a (J)	ΔH_{sil} (J)	ΔH_{conv} (J)	ΔH_{rad} (J)	E_{req} (J)	E_i (J)
5	82.3	83.4	64.9	57.4	288.1	409.4
10	82.3	83.4	6.8	7.4	180.0	215.2
15	82.3	83.4	2.1	3.0	170.8	218.1
20	82.3	83.4	0.8	1.5	168.0	208.6

Table 2.2: The various enthalpic energies required for activation at several voltages on four sample devices. Greater heat (ΔH_{total}) is required at lower voltages because there are greater losses to convection (ΔH_{conv}) and radiation (ΔH_{rad}). As a result, more electrical energy (E_i) is required; however, this increase is not perfectly predicted by the increased heat, as a result of various losses not considered in this analysis.

we see that the see that this input is somewhat underpredicted by these equations.

Nevertheless, these equations serve as a useful way to estimate energy consumptions for various voltages and conditions. This under-prediction arises from several possible sources:

1. There is more energy stored in the silicone than predicted. As the cTP heats, a temperature gradient between the cTP and the free surface arises. We only measure the temperature at the surface, neglecting the heat stored closer to the cTP element.

2. There is radiation and convection from all six surfaces, though we assume these phenomena occur only on the sides with the largest area.

3. We ignore the added heat sinks from the EGaIn electrodes and copper leads.

4. Some of the measured power is dissipated through the circuit wires, rather than through the cTP element.

Finally, we note that there are considerably fewer losses to convection and radiation at higher voltages, since the activation time is much shorter.

2.4 Stiffness Change Response Experiments

We investigated three components of the stiffness change response: the switching ratio (i.e. the ratio between the modulus in the stiff state and the modulus in the soft state), activation time, and the recoverability (i.e. the ability of the stiffness switch to regain its original shape after deformation). The stiffness switches were loaded on a universal testing machine (Model 5969,

Instron) using 3D-printed clips. Both the top and bottom clip supported a screw that passed through the unactivated portion of the Ecoflex and cTPE, so tension could be applied directly to the cTP. To find the switching ratio, each device was repeatedly loaded between 0 and 2.5% strain at a rate of 0.5 mm s^{-1} in both the high- and low-stiffness states. An effective modulus was calculated for each state by averaging the slope of the loading and unloading stress-strain curves. These tests revealed two distinct stiffness states: a rigid state with modulus E = 10.4 MPa ± 0.5 MPa and a soft state with modulus E = 0.7 MPa ± 0.08 MPa - a switching ratio of 14.9 (Figure 2.5 A).

To determine their recovery behavior, each switch was actuated and deformed to increasingly larger strains in increments of 10% (Figure 2.5 B). Between each test, a new natural length was measured, and the test was repeated until failure, as defined by 1) the inability to heat to activation or 2) the initiation of tearing in the cTP[7]. These tests reveal that the stress-strain behavior of the soft-state switches at high strain (40%) is similar to their behavior at low strain (2.5%) (Figure 2.5 A). Additionally, because of the high viscosity of the melt-state cTP, the switches exhibit some change in their natural length after high strain. However, after several minutes, the switches retain only 1 or 2 mm of permanent deformation, thanks to the elastic restoring force of the silicone casing. These findings indicate that these stiffness switches may be useful in applications requiring up to 40% of axial deformation.

We also measured the current in the stiffness switch over large strains. Since the electrical resistance of a through-thickness composite is inversely related to its thickness, a switch experiences a dramatic drop in resistance as it is deformed, resulting from the thinning in the

[7] Although the switch's activated state corresponds to the melt state of the cTP, excessive strain can cause tearing in the stiffness-tuning element, known as melt fracture.

stiffness-switching element caused by the Poisson effect. This can yield a large increase in the heating rate, which may place the composite at risk for thermal damage. However, as the temperature rises, the cTP resistance increases, due in part to the thermal expansion of the polymer, which increases the distance between the carbon black particles, and thus the resistivity of the composite[111,112]. This added resistance reduces the applied current, and creates a stabilizing negative feedback loop, that can be seen in the leveling off of the current after a

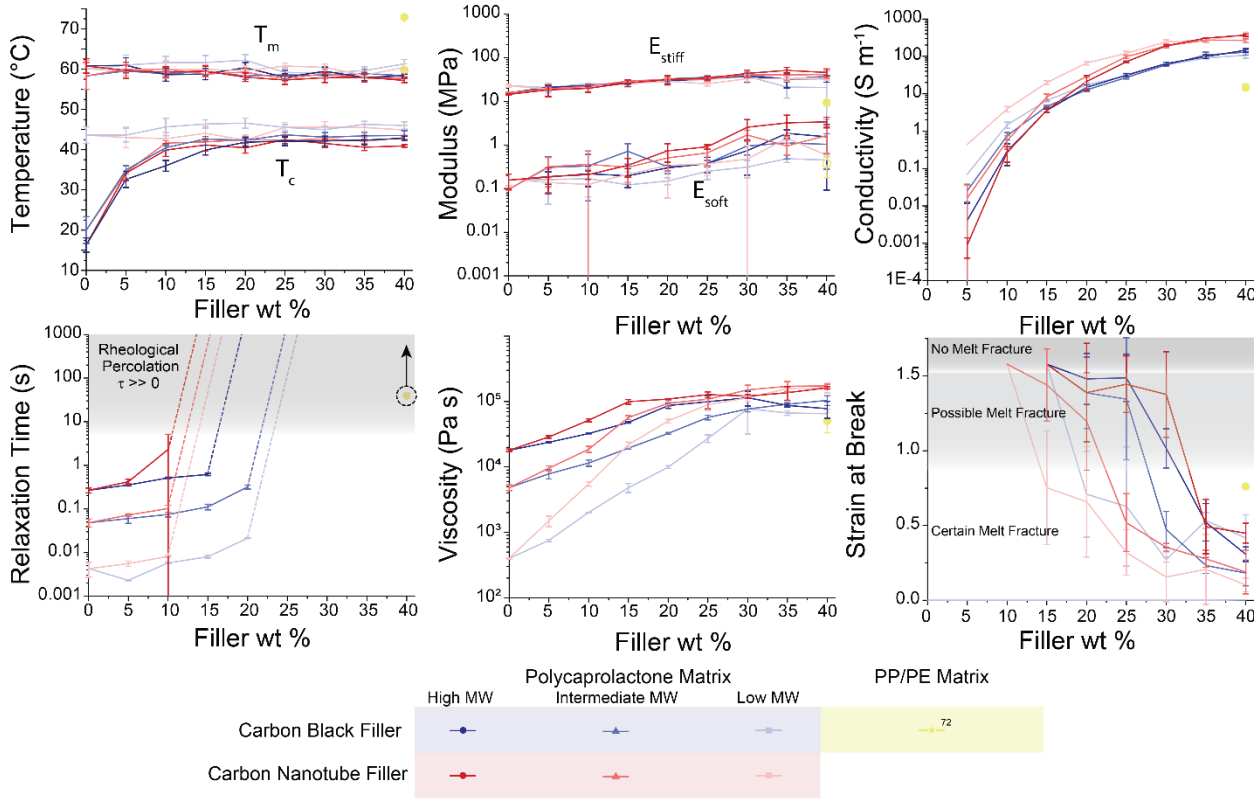

Figure 2.5: Actuation response of a cPBE stiffness switch. (A) Stress-strain behavior for the extension and contraction of a switch in both the stiff and the soft state. (B) The recoverability of a switch as it is extended to increasingly larger strains. (C) The current as a function of strain for three samples taken to failure. (D) The decline in applied stress ① as a function of time during activation ②. (E) The activation time for switches under various applied voltages, when activation is considered as 90% of the maximum drop in modulus (green) or 50% of the maximum drop in modulus (brown). (F) The stress strain behavior of unpatterned and patterned cTPE tendons, demonstrating the potential for tuning the preactivation stiffness.

certain strain value (Figure 2.5 C).

The activation time was measured by preloading each switch to 75 kPa and applying a voltage between 5 V and 20 V, while measuring the decline in stress over time (Figure 2.5 D). This decline manifests as a negative sigmoid curve, approaching an asymptote as the composite becomes fully melted and the switch relaxes. Thus, we define the activation time, t_a as the time at which the switch modulus has decreased 90% of its total drop. Both the activation time and the maximum temperature are highly dependent on the voltage applied across the composite, since the energy input to the system rises with the square of the voltage (Equation 2.7). At 5 V, the stiffness switch becomes soft in approximately 40 s, while at 20 V, it takes less than 2 s (Figure 2.5 E).

Finally, we demonstrate that the maximum stiffness of the device can be tuned via patterning. The cTP composite was cut using a UV laser cutter (ProtoLaser U3; LPKF), and the stress-strain response was measured[8].

2.5 Demonstrations

The abilities of these cTP-based stiffness switches are demonstrated with two illustrative use cases. In the first demonstration, we demonstrate an articulated finger model that can achieve two bending modes from a single string-based actuator, by employing a cTP-based active tendon at the proximal joint and a passive silicone rubber tendon at the distal joint (Figure 2.6 A). When the tendon is unactivated, the stiffness at the cTP-based tendon is an order of magnitude higher than that at the pure silicone tendon, allowing bending at the distal joint while preventing

[8] Tensile tests were performed by Dr. Sung-Hwan Jang (Plymouth University).

bending at the proximal joint. When the tendon is activated, the stiffness at the proximal tendon becomes similar to that of the pure silicone tendon, resulting in bending at both joints when tension is applied to the string. Because the stiffness of the soft-state cTP-based tendon is still higher than that of the pure silicone tendon, bending occurs at the distal joint first.

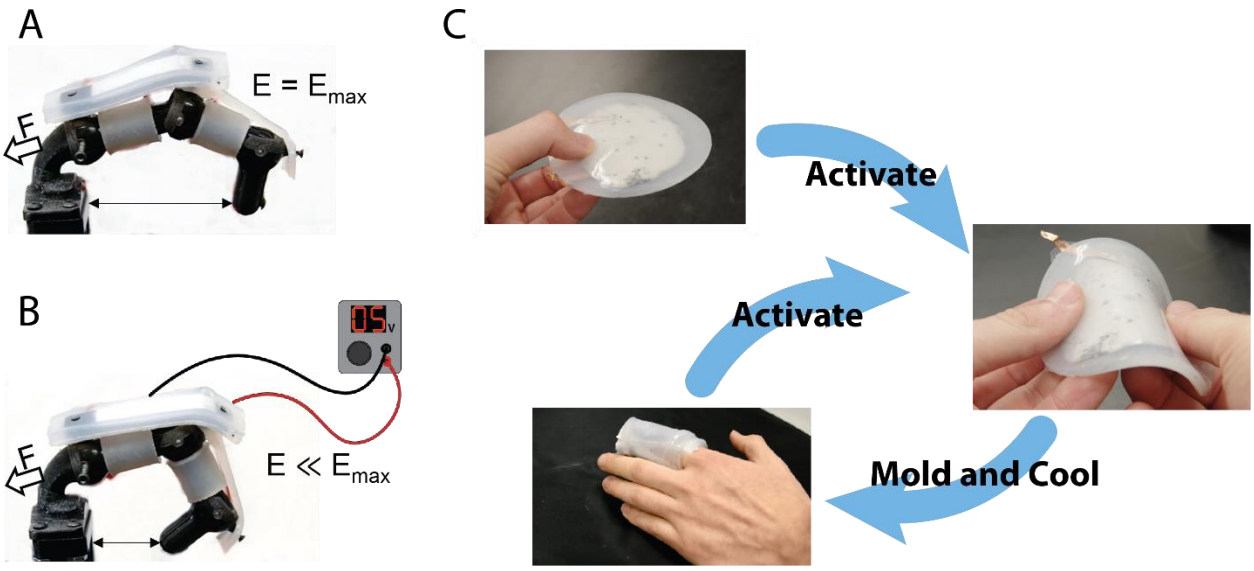

Figure 2.6: cTP incorporated into a robotic and wearable application. (A) Gripping configurations with an unactivated tendon (top) and an activated tendon (bottom) (B) A voltage-activated moldable splint, enabled by a cTPE sheet.

We also demonstrate the versatility of through-thickness cTP-based actuation for wearable medical applications. Splints have been widely used to treat conditions that require joint immobilization, such as osteoarthritis or ulnar collateral ligament tears[113]. For decades, these devices have incorporated thermoplastics to allow patients to conform them to their body, and reshape them if they experience discomfort[114]. Applying the heat necessary to soften the thermoplastic, however, requires bulky or specialized equipment like heat guns or water baths that make on-the-go adjustments impractical. To provide portable, reversible stiffness tuning we incorporate a cTP-based stiffness-switching sheet into a moldable stiffness-switching splint

(Figure 2.6 B). Previous direct heating stiffness-tuning methods[74,86] had activation areas that were restricted to the shortest linear path between two electrodes, making it difficult to tune the stiffness of sheets. By orienting the electrodes across the full face of the cTP, we make the entire surface area the shortest path between the electrodes, allowing us to activate any arbitrary cTP geometry. When a voltage is applied across the two electrodes, the cTP sheet melts, transitioning from a stiff, elastic state to a soft, moldable state that is capable of conforming to a patient's hand. A silicone wrap helps secure the compliant sheet and ensure its proper configuration. Once the sheet has been applied to the target area, the voltage is removed and the sheet returns to its stiff state, functioning as a splint. Although the cTP must surpass 72.9 °C for activation, it is insulated from the skin with a layer of stretchable nylon fabric.

2.6 Conclusion

In this chapter, we develop a stiffness switch based on a conductive low-melting-point thermoplastic. The novel through-thickness activation scheme reduces the required activation time and voltage and enables the stiffness switching of arbitrary geometries. With these devices, we show a competitive switching ratio, good recoverability, and controllable actuation behavior. We also investigate the activation mechanism of cPBE through DSC and DMA, and provide a model relating these thermal properties to the energy required for activation. Finally, we present two demonstrations, an active robotic tendon and a remoldable splint, based on the stiffness-switching method developed. Although these applications display the potential for cTP-based stiffness switching in soft robotics, they also reveal specific weaknesses in the thermoplastic composite used.

High Melting Point Though activation times can be reduced to under 2 s by adjusting the power delivered to the cTP, deactivation times remain dependent on the dissipation of heat. Because of the high melting point of cPBE, these deactivation times are long, on the order of minutes. For some applications, such as splints, this may be desirable, but for robotic actuation, such as the tendon presented in Figure 2.6 A-B, this may pose a problem. Additionally, because the temperatures attained by devices can be uncomfortable, wearables may require insulation to protect users.

Low Extensibility We demonstrate elastic strain of >40% in stiffness switches in the soft-state. Above this strain, however, stiffness-switching elements are likely to experience melt fracture, causing electrical and mechanical failure. For many robotic applications, including the stiffness-switching tendon presented in this chapter, this maximum strain value may be insufficient. Although most tendons incorporated into the finger were able to withstand these extensions, many of the stiffness-switching elements experienced melt fracture when deformed in the melt state.

Limited Conductivity Choice In previous work[86], these composites required high activation voltages as a result of their high resistivity. Reconfiguring the electrodes into a through-thickness orientation circumvented this problem, while enabling the activation of arbitrary geometries. As these geometries increase size, however, the cTP resistance decreases as a function of area: $R = \rho L/A$, where ρ is resistivity, L is conductor length, and A is conductor area. Therefore, for large devices, the resistance may drop to less than that of the wires delivering current, causing heating in the wires. Different applications that require different cTP areas, thus, may require different cTP resistivities.

In short, the requirements of a stiffness-switching device vary significantly with the desired

application. Figure 2.7 shows the which properties may be desirable for specific use cases, while Table 3 shows a more specific use case for of each property. In order to improve the relevance and functionality of cTP-based stiffness-switching devices, we seek to control these factors by examining the cTP composition in detail in Chapter 3.

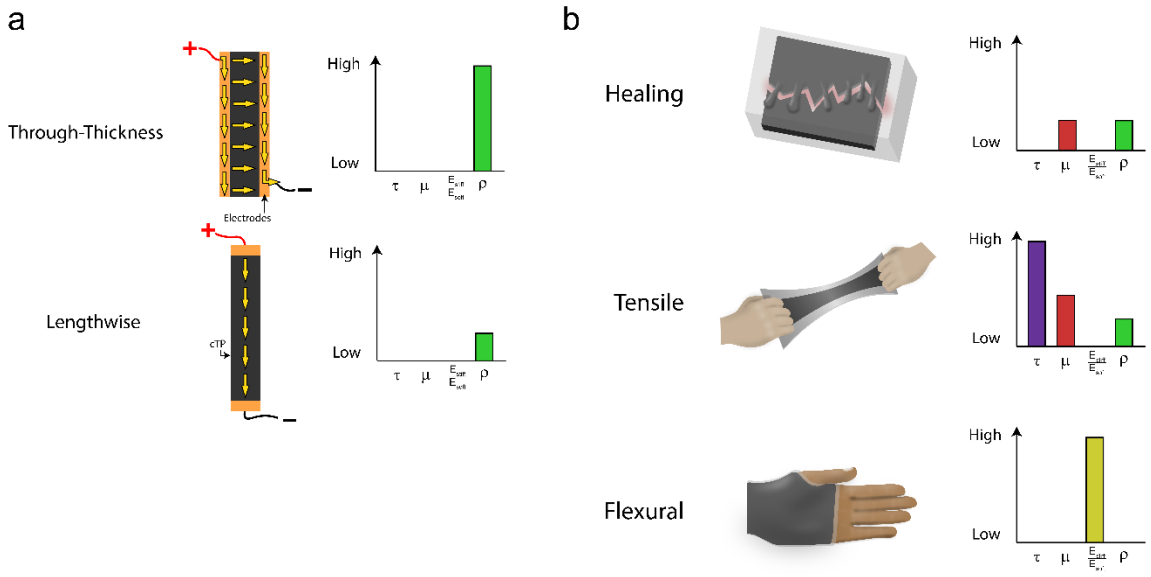

Figure 2.7: Required mechanical, rheological, and electrical properties for general stiffness-switching modes. A) Two electrode layouts: through-thickness, which requires a high composite resistivity, lengthwise, which requires a low composite resistivity. B) Three classes of application: healing, tensile, and flexural modes, which require a different mix of properties to achieve maximum performance.

Parameter		Utility	Importance for Tensile Applications	Importance for Flexural Applications	Importance for Self-Healing Applications	Other Notes	
Melt-State Strain Limit	High	Applications that experience high positive strain	**HIGH** Small axial deflections yield significant strain in tensile loading	**MEDIUM** Large bending deflections yield relatively small tensile strain in flexural loading	**IRRELEVANT** Does not experience any tensile strain		+
	Low	Applications where fracture at certain strain is desirable	Variable	Variable	Variable		-
Switching Ratio	High	Applications where small strain must be accentuated by large change in rigidity	**MEDIUM** Small axial deflections yield significant strain, for which large changes in stiffness are readily apparent	**HIGH** Large bending deflections yield relatively small strain, which must be accentuated	**LOW** Must only be soft enough to be compressed in soft state, able to maintain its shape in stiff state		+
	Low	Applications where stiff and soft state should be similar	Variable	Variable	Variable		-
Viscosity	High	Applications where damping or slow stress-relaxation/creep is desired	Variable	Variable	Variable		-
	Low	Applications where strain rate is high, allowable hysteresis is low, or flow is desired	**MEDIUM** Small axial deflections yield significant strain, which may correspond to a high strain rate	**LOW** Large bending deflections yield relatively small strain, which may correspond to a low strain rate	**HIGH** A high flow rate allows two halves of composite to reform under minimal pressure		+
Conductivity	High	Applications where a high current and low voltage is desired; applications where fast activation is desired	Variable	Variable	**MEDIUM** Since high resistence occurs at interface between composite halves, high composite conductivity allows sufficient current to flow for activation	**Desirable for Lengthwise Actuation** Since geometric parameters reduce conductance, higher conductivity allows for lower voltages	
	Low	Applications where a low current and high voltage is desired; applications where slow activation is desired	Variable	Variable	Variable	**Desirable for Through-Thickness Actuation** Since geometric parameters increase conductance, low conductivity limits current to safe levels	
Melting Temperature	High	Applications where accidental actuation because of high ambient temperatures is a risk	Variable	Variable	Variable		-
	Low	Applications where low activation energies or safe temperature levels are desired	Variable	Variable	Variable		+
Thermal Hysteresis	High	Applications where long restiffening times are desired	Variable	Variable	Variable		
	Low	Applications where short restiffening times are desired	Variable	Variable	Variable		

Figure 2.8: The effects of various properties of a cTP composite on the overall behavior of a device tailored to a tensile, flexural, or healing application.

3
Tuning the Properties of Stiffness-Switching and Electrically Healable Composites[9]

3.1 Background

Thermoplastics are important commodity materials that are used in many diverse industrial and consumer applications. Mixing these materials with different nanoparticle fillers can yield new composites with improved mechanical, rheological, thermal, or electrical properties, that are important to a variety of applications including photovoltaics, strain sensing, supercapacitors, electromagnetic interference shielding, and water purification[115,116]. Although these composites are relatively new additions to the field of stiffness-switching, they have been extensively studied in other fields.

Conductivity of Thermoplastic Nanocomposites There is a well-established body of work investigating the relationship between the concentration of conductive filler in a polymer nanocomposite and its conductivity[117]. Conductivity can be established in these systems when conductive filler (e.g. carbon nanotubes, carbon black) forms a percolating network, where the particles are either touching or are close enough to allow for electron tunneling through the polymer[118,119,120,121,122,123]. The minimum concentration of filler at which conductivity occurs, known as the **electrical percolation threshold**, is an important parameter for these systems, and can be lower than 0.019 vol%[124]. This threshold, along with the filler concentration-

[9] This work was completed in collaboration with Vasudevan Nambeesan, Rehan Khan, and Professor Carmel Majidi.

conductivity relationship varies dramatically with the polymers, fillers, and processing conditions[117]. Often, the conductivity of a composite can be improved by employing high-aspect ratio fillers like carbon nanotubes, or by manipulating filler dispersion[115,125]. Above the percolation threshold, a greater filler concentration generally yields higher conductivity according to the power law relation: $\sigma \propto (m - m_c)\beta_0$, where σ is the electrical conductivity, m is the filler mass fraction, m_c is the electrical percolation threshold, and β_0 is the critical exponent[126].

Rheology of Thermoplastic Nanocomposites Since thermoplastics are generally processed and shaped in the melt state (e.g. extrusion, injection molding), their rheological properties are critical to the manufacturability. As a result, there have been a wide variety studies investigating polymer melts and solutions, and the effects of fillers on their properties, including viscosity[119,127,123,128,126,129], melt fracture[130,131,132,129], rheological percolation [133,122,123,119,134,127,126,128,112], and relaxation time[135,127,132,129].

As with electrical percolation, there exists a filler concentration above which **rheological percolation**, or gelation, occurs. This phenomenon arises from the formation of a filler network within the nanocomposite; however the relationship between this network and that required for electrical percolation can vary[127,123,126,119]. When the rheological percolation threshold is *below* the electrical percolation threshold, the filler particles can act as entanglements in the polymer chain when the distance between filler particles is still too great to allow for electron tunneling[126,123]. When the rheological percolation threshold is *above* the electrical percolation threshold (known as a "rigid" rheological percolation, the filler is capable of forming an initial conductive cluster formed without impeding the mobility of the polymer chains[123]. The storage modulus (*G'*), the inverse loss tangent (*G'/G"*), and the complex viscosity (η^*) have all been

suggested as parameters to represent rheological percolation, though a degree of subjectivity is often involve[119,123,136].

Other Properties of Filled Polymer Fillers have also been widely incorporated into polymers to improve the mechanical, thermal or dielectric properties[115]. These materials can increase the modulus or strength of polymer[137,115] nanocomposites, and act as a nucleation promotor or inhibitor to depress or increase the melting and crystallization points of the system[128,138,115,112].

However, despite this extensive literature, no work has yet examined these properties in a regime relevant to stiffness-switching composites. In this work, we investigate the effects of filler type, filler concentration, and matrix polymer molecular weight on the critical properties of the stiffness-switching material. Using these parameters, we develop a composition selection guide, which we use to construct three different stiffness-switching applications: a highly extensible stiffness-switching tendon, a large-area moldable sheet, and an electrically healable mechanical fuse.

3.2 Characterization of cPCL Composites

Sample Preparation Polycaprolactone (PCL) of three different molecular weights (CAPA 6800: M_w = 88 400 g mol^{-1}, CAPA 6500: 55 500 g mol^{-1},CAPA 6250: 28 900 g mol^{-1} [129]) from Perstorp AB were used as the matrix material for the stiffness-switching element. PCL was selected for its low melting point, which decreases the energy required to initiate melting and increases the safety of the associated device. The filler materials used were carbon black (acetylene, 100% compressed, Alpha Aesar) and multi-walled carbon nanotubes (Outer Diameter: 50 nm–80 nm, Length: 10 μm–20 μm; Cheap Tubes).

To create sheets of conductive PCL, the pellets of PCL were added to a mixture of toluene

(anhydrous, 99.8%, Sigma Aldrich) and conductive filler and stirred for at least 3 hours at 50–80 °C on a magnetic stirring plate (Figure 3.1). The total mass of PCL and filler was 10 g, with filler loading fractions ranging from 0-40% filler by weight. A sufficient volume of toluene was used to create a uniform dispersion of filler in polymer solution (50 mL–70 mL). The mixture was poured into a large petri dish (150 mm × 25 mm, DURAN Group) and left overnight for the solvent to evaporate. The resulting sheets were compressed on a heat press (Model C 3912, Carver) under 1000 lbs at 80 °C in an aluminum mold 1.3 mm thick. Once solidified, these sheets were cut into the desired shape using a 30 W CO_2 laser cutter (VLS 3.50, Universal Laser Systems), and cleaned with all-purpose cleaner (Simple Green).

Figure 3.1: Procedure for the preparation of conductive PCL sheets. **Step I:** PCL pellets are added to a mixture of carbon filler and toluene, and stirred until the mixture becomes homogeneous. **Step II:** The mixture is poured into a large petri dish and the solvent is allowed to evaporate. **Step III:** The resulting conductive PCL is compressed with a heat press to create a flat homogeneous sheet.

Thermal Characterization The thermal properties of the cTP composite have a significant influence on the stiffness and phase-transitioning behavior of the stiffness switch. The melting temperature (T_m) and crystallization temperature (T_c) of the cTP composite control the stiff-soft transition points, while the specific heat capacity and the specific latent heat of fusion of the

composite determine the amount of electrical energy required to soften a given switch. A low melting point and specific heat improve the activation time (i.e. the time required for the switch to soften) and lower the energy cost of switching; however, these values must be high enough to prevent accidental softening in ambient conditions. Similarly, the magnitude of the difference between the crystallization and melting temperatures corresponds to the deactivation time (i.e. the time required for the composite to restiffen). Engineers may wish to minimize or maximize the time for this transition depending on the application.

Differential scanning calorimetry (DSC) experiments reveal a melting temperature that is very consistent (≈ 60 ◦C) across all molecular weights, fillers, and loading fractions (Figure 3.2A). It is 13 °C lower than the transition temperature for cPBE, which indicates a potential improvement in the safety, speed and efficiency of a stiffness switch. The crystallization point for most of the composites tested is around 44 °C, which is 16 °C lower than the melting temperature, indicating a significant wait time for restiffening. This asymmetry is typical of polymer systems, including cPBE, and may be useful for maintaining a device such as a splint in the soft state without applying power, while it is shaped to the body. At low filler loading fractions, the crystallization temperature decreases dramatically for the high and intermediate molecular weight conditions, indicating an even longer stiffening transition. The filler, in this case, seems to function as a nucleation promoter for longer chain polymers, which may not form crystal structures as easily[138]. Thus, while minor adjustments to the crystallization temperature may be made by adjusting the composition, more substantial control over thermal properties should be achieved by employing alternative base polymers.

Modulus Measurements For applications in active garments and soft robotics, it is important to

characterize the Young's modulus of the material in both its soft and stiff states. A high ratio between these moduli is often desirable to maximize stability in the stiff state and maximize compliance in the soft state.

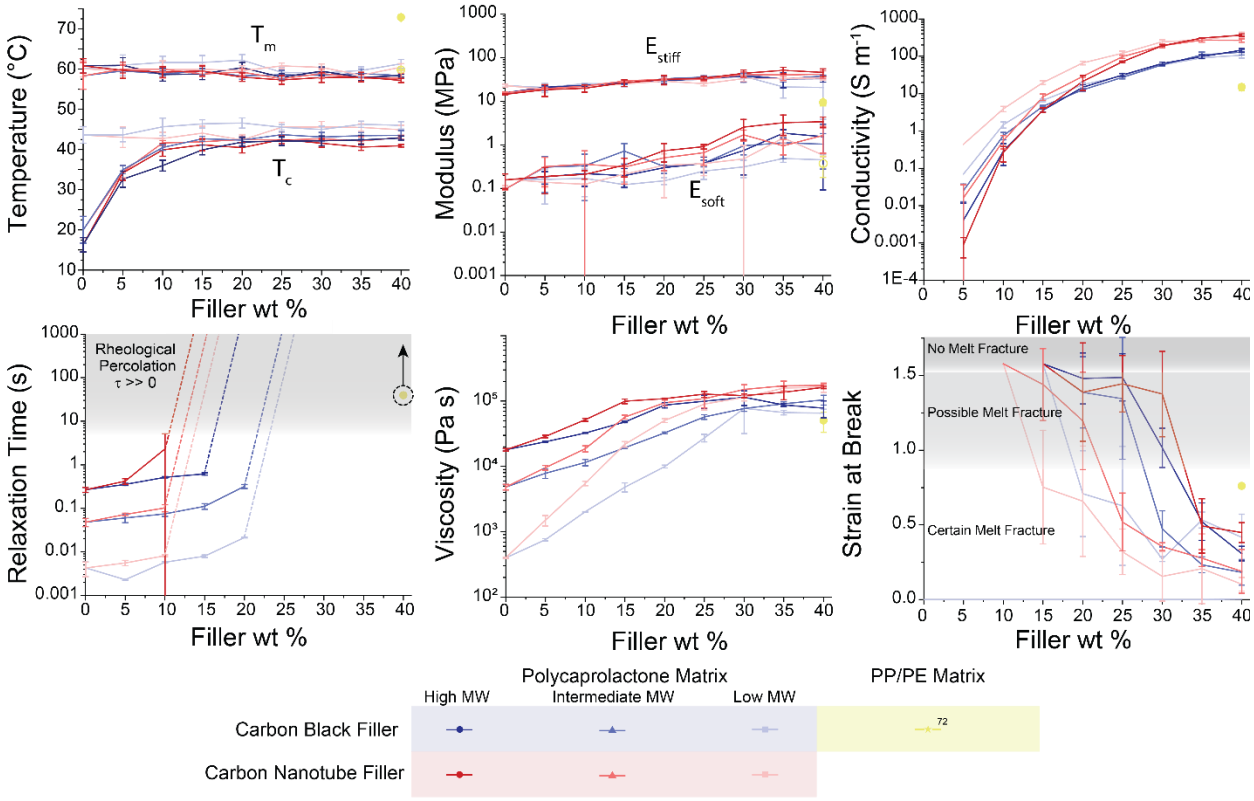

Figure 3.2: Properties of conductive thermoplastic polymers as a function of matrix material, filler type, and filler loading fraction (wt %). (A) The relationship between melting point T_m (upper lines, filled symbols) and crystallization point T_c (lower lines, open symbols) and filler loading fraction. (B) The relationship between stiff-state modulus E_{stiff} (upper lines, filled symbols) and soft-state modulus E_{soft} (lower lines, open symbols) and filler loading fraction. (C) The relationship between conductivity and filler loading fraction. (D) The relationship between relaxation time τ and filler loading fraction. (E) The relationship between dynamic viscosity μ and filler loading fraction. (F) The relationship between melt-state strain-at-break and filler loading fraction.

Stiff-state modulus measurements show a modest increase in the stiffness of composites with higher filler loading fractions (Figure 3.2 B), as is typical for filled polymer systems[137]. Soft-state modulus measurements also show a modest increase in stiffness as loading fraction rises,

likely due to the increase in the storage modulus, *G'*, seen in the rheology measurements. This is also reflected in the reduced soft-state stiffness in lower molecular weight composites.

The ratio between the modulus of the stiff state and the soft state, known as the switching ratio, decreases significantly as filler loading fraction increases. At low loading fractions, the switching ratio varies from 37-207, representing a dramatic increase over that found in cPBE (max switching ratio: 24)[86], and is competitive with other stiffness switching methods[18]. However, since there is significant noise associated with the soft-state measurements and thus the switching ratio, we recommend controlling the switching ratio and modulus bounds through other methods (e.g. geometrical considerations (Figure 2.5 F) and base polymer selection).

Conductivity Measurements The bulk conductivity defines the resistance of the stiffness-switching element, which impacts the the voltage, the current, and the time required for activation. A high conductivity reduces the required voltage and activation time, while increasing the associated current[85].

At high filler loading fractions, the conductivity for all composite molecular weights converges to a single value corresponding to the filler material (Figure 3.2 C). In agreement with previous studies, carbon nanotube-filled composites have significantly higher conductivity than those filled with carbon black, because their high aspect ratio increases the structure of the percolating network[125]. Furthermore, their lower density[139] may lead to higher volumetric loading for the same weight percent, which would cause a denser percolating network.

At lower filler loading fractions, the conductivity of the composites shows a greater

dependence on polymer molecular weight, where low molecular weight composites have a higher conductivity. This is likely due to the longer polymer chains disrupting the structure of the percolating network. For all molecular weight and filler combinations, the conductivity of carbon-PCL composites is significantly higher than the conductivity of the cPBE at comparable loading fractions. In fact, the same conductivity can be achieved with filler loading fraction as low as 15% for carbon-PCL composites.

Since the filler loading fraction has a strong influence on the mechanical and rheological properties of these composites, decreasing the loading fraction can have a favorable effect on stiffness-switching behavior, by increasing stiff-state flexibility and decreasing melt-state viscosity.

Rheological Measurements

The rheological properties of cTP govern the mechanical behavior of the stiffness-switching element in the soft-state. The viscosity, for instance, can affect both the ease by which a stiffness switch in the soft state can be deformed and its plasticity, while the relaxation time can serve as a proxy for measuring the risk of tearing for a stiffness-switching element in the soft state. The likelihood of tearing, or more specifically melt fracture, becomes significant when the Weissenberg number, defined as the product of relaxation time τ and strain rate $\dot{\varepsilon}$ ($Wi = \tau\dot{\varepsilon}$) exceeds a critical value[131,132]. Therefore, low viscosities and relaxation times are desirable for maximizing the elasticity and softness of the composite in the soft state, while high viscosities can help maintain the mechanical stability of a device in the soft state, useful for shape-locking applications.

We find higher relaxation times for composites with high molecular weight (Figure 3.2 D), corresponding to the empirical relationship found in the literature $\tau \sim M^{3.4}$[140], where τ is relaxation time, and M is molecular weight (Figure 3.3). There is also an increase in relaxation time associated with an increase in filler (which is common for many polymer-filler systems[135,119]) that for this work corresponds to a decrease in the goodness-of-fit.

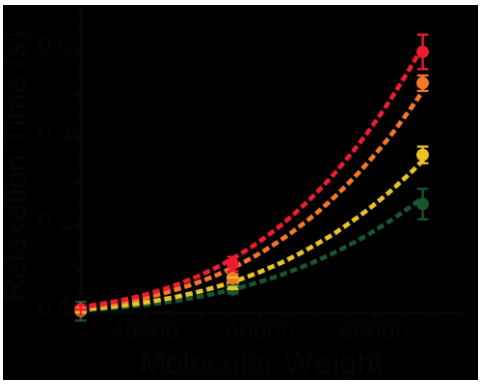

Figure 3.3: Relaxation time as a function of molecular weight for carbon black-filled cPCL composites. The dashed lines represent the fit provided by the equation shown. Carbon nanotube-filled composites show similar behavior.

For all filler and molecular weight combinations, there is a specific loading fraction above which we observe a sudden increase in relaxation time[133,119]. Above this loading fraction, the relaxation time of the melted composite cannot be measured over reasonable timescales and temperatures. Since relaxation time τ corresponds to the point where $G'/G'' = 1$, this critical point reflects the rheological percolation threshold, above which the material may behave as a pseudosolid[119,127]. This jump in relaxation time yields a corresponding jump in the Weissenberg number, which can be used to indicate the loading fraction above which melt fracture is likely to occur. When compared with previous work, rheological percolation in these composites occurs at significantly higher loading than other systems[123]. Furthermore, these composites are, to our knowledge, the only stiffness-switching conductive polymers below rheological percolation.

Unlike relaxation time, viscosity does not increase beyond the limits of the rheometer at the rheological percolation threshold, allowing us to measure the melt-state behavior of high-loading-fraction composites (Figure 3.2 E). The viscosities increase quickly as filler is initially

added to the PCL composites, and approach an asymptote at higher loading fractions. For an equivalent polymer matrix, composites with carbon nanotube filler have a higher viscosity than those with carbon black, because the interactions between anisotropic filler play a larger role than those between isotropic filler. Additionally, polymers with a higher molecular weight inherently have a significantly higher viscosity. This indicates that independent control of viscosity, conductivity, and relaxation time cannot be achieved by controlling the given parameters. However, composites with a range properties exist within the design space, allowing for the selection of a specific composition for a desired application (Figure 3.4).

Furthermore, as the viscosity of the composite increases, the ability of the composite to regain its original shape becomes more dependent on the rate at which the strain is reduced. For some

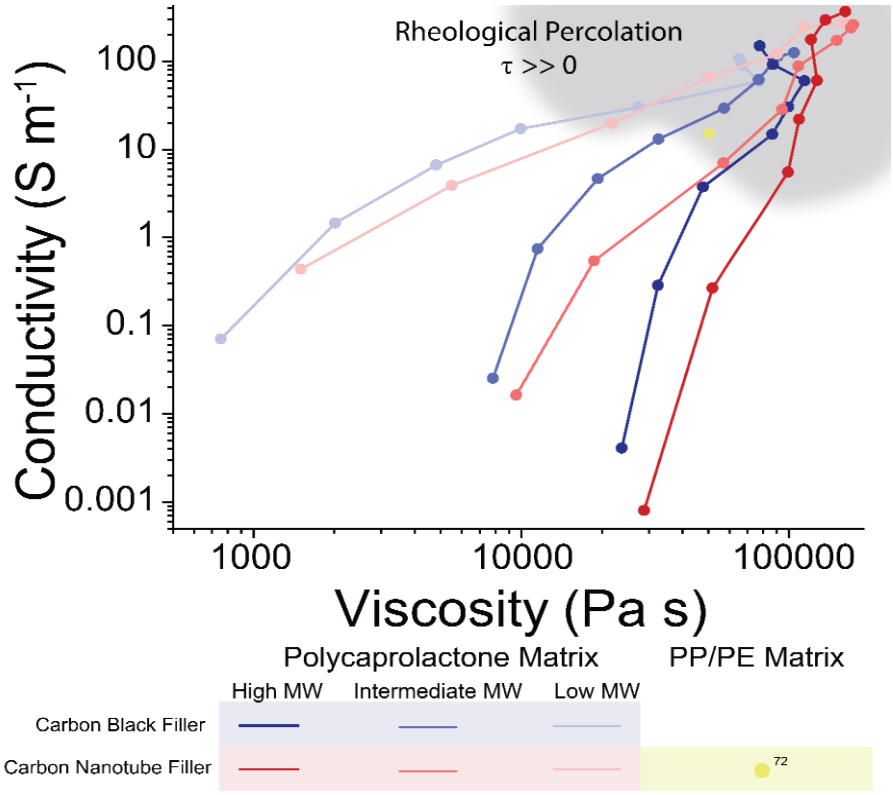

Figure 3.4: The design space for the cTP composites tested, including conductivity, viscosity, and relaxation time.

composites with intermediate filler loading fractions, buckling or plastic deformation may occur if they are returned to their initial shape too quickly. Therefore, the expected unloading speed is an important consideration when selecting the viscosity of a stiffness-switching device. The precise relationship between unloading speed and shape recovery is the subject of future work.

The melt-state strain-at-break determines the viability of a composite for use in stiffness switching applications that require significant extensional strain in the soft state. Composites with high filler loading fractions typically experience melt fracture at lower strain values (Figure 3.2 F). At low filler loading fractions, the composites become less likely to experience melt fracture even at large strains. The critical loading fraction above which melt fracture occurs corresponds roughly to the rheological percolation value shown in the rheology tests (Figure 3.2 D). This indicates that rheological percolation can serve as a useful metric to determine the suitability of various formulations to extensional stiffness switching applications. However, because these tests more closely reflect real-life actuation than standard melt-fracture tests, they are subject to more stochasticity, which can be associated with premature or even delayed melt fracture. This is reflected in the discrepancies between the melt fracture (Figure 3.2 F) and relaxation time (Figure 3.2 D) plots, as well as the large error bars in Figure 3.2 F. Interestingly, at filler loading fractions above this critical loading, composites with higher molecular weight can withstand a greater strain before melt fracture than composites with lower molecular weight. This is somewhat counterintuitive since these composites have a higher relaxation time; however, because the applied strain rate is relatively slow, this behavior may be explained by greater stability provided by longer polymer chains.

Because of the elongated shape of their filler, carbon nanotube-based composites may show dramatic changes in electrical and rheological properties during extension, as the carbon

nanotubes start to align along the direction of strain[108].

3.3 Demonstrations

The wide variety of properties achievable with carbon-PCL nanocomposites make these composites well-suited to diverse applications, including tensile stiffness switching, flexural stiffness switching, shape-locking, and electrically activated healing (Figure 3.5 A-C). We show each of these behaviors in three illustrative demonstrations, with stiffness-switching devices

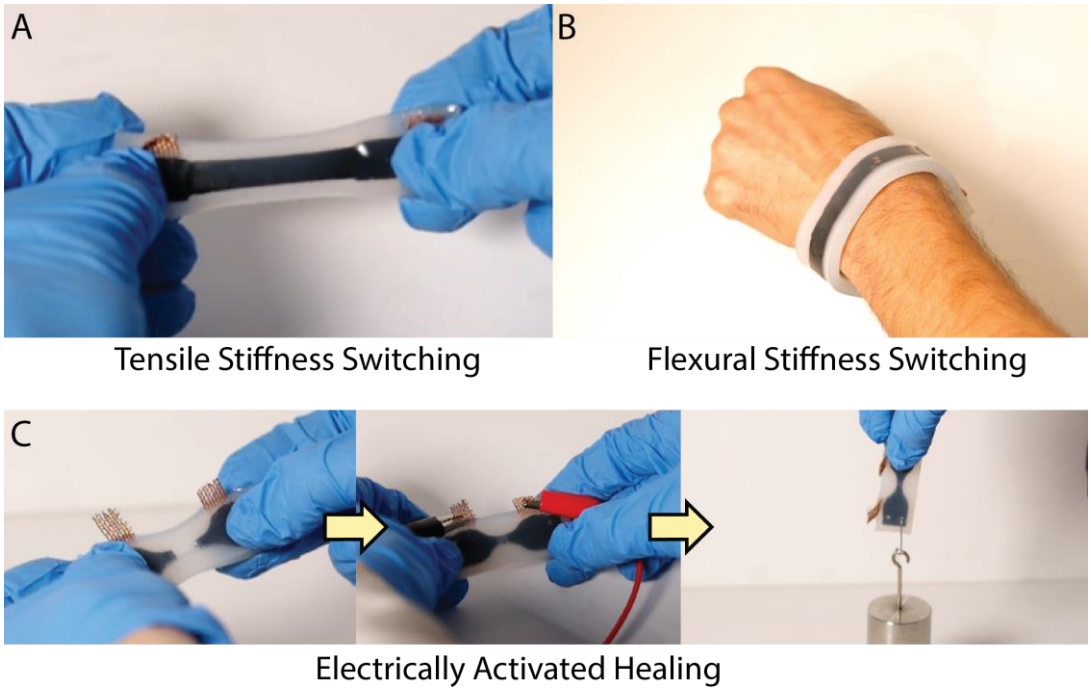

Figure 3.5: Demonstrations of activation modes for cPCL devices, including: (A) lengthwise-activated tensile stiffness-switching, (B) through-thickness activated flexural stiffness-switching and shape-locking, and (C) lengthwise-activated healing.

based on different composite formulations.

Tensile Stiffness-Switching Tendon[10] The first demonstration shows a stiffness-switching tendon for use in soft robotic systems undergoing large tensile deformations. To accommodate these large deformations, the electrodes were oriented for lengthwise actuation, as highly stretchable electrodes capable of interfacing with conductive thermoplastic have not yet been demonstrated. A lengthwise activation scheme requires a high conductivity and a high voltage (30 V), while a tensile deformation mode requires a high stretchability (Figure 2.7). Therefore, we select the highest conductivity composite below rheological percolation that also has a low viscosity (Figure 3.4), a low-molecular weight PCL filled with 20% carbon black. Lower conductivity composites could be used in order to achieve very large deformations with very little plastic deformation if a higher voltage were applied.

Flexural Stiffness-Switching Strip[11] The second demonstration shows a shape-locking stiffness-switching strip for use in splints and other body-conforming wearable devices. Because the primary mode of deformation is flexural, the stiffness ratio should be high, which is guaranteed by most carbon-PCL compositions with low-to-moderate loading fractions. Because the sheet comprises a large actuation length, lengthwise actuation would require a very high

[10] The tensile stiffness-switching tendon demonstration was completed with the help of Dr. Eric Markvicka.

[11] The stiffness-switching strip was developed by Vasudevan Nambeesan and Rehan Khan under my guidance. The demonstration was completed together with Vasudevan Nambeesan.

voltage for most composite compositions; therefore, the electrodes are oriented for through-thickness actuation. For the intermediate activation area selected, this choice of electrode position requires a composite with intermediate conductivity. Additionally, since shape-fixing requires high soft-state stability without brittleness, the cTP must have an intermediate viscosity. Therefore, we select an intermediate-molecular weight composite with 15% carbon black (Figure 3.4).

Additionally, because the entire device experiences bending in the soft state, the electrode material must be both compliant and highly conductive. We select a fine copper (200 per in., 0.002 in. wire diameter, TWP Inc.) mesh, and embed it on either side of the cTP strip. Although we are able to achieve significant softening with this configuration, the soft-state behavior highlights the need for improved electrode materials. The electrodes used here cannot stretch as required for bending and undergo some plastic deformation at large strains. This mismatch manifests in the flexural stiffness switch via surface rippling that occurs after bending.

Electrically Healable Mechanical Fuse[12] The third demonstration shows a mechanical fuse that can be electrically healed (Figure 3.6). Healable materials are important for future soft robots since these devices are susceptible to damage[141]. Alternatively, these devices could be used to limit the maximum force of a soft robot to a desired level. To demonstrate this behavior, the cTP fuse is first broken in the center. The elastic casing returns the two fragments to their original position and a small compression is applied, placing them superficially in contact. Because the contact resistance between these two parts is higher than the bulk resistance of the cTP, heating

[12] The electrically healable mechanical fuse demonstration was completed with the help of Dr. Eric Markvicka.

occurs at the interface when 30 V is applied across the fuse for approximately 6 s. As the composite melts, the polymer chains re-entangle, allowing the composite to recombine upon cooling, healing it mechanically and electrically. Tensile tests conducted after healing reveal that the composite retains 65% of its original strength (Appendix 5.2). Because of its low melting point, PCL has already shown promise in healable electronics and shape-memory materials[108,142]; however, electrically induced healing has not yet been demonstrated. To allow the fuse to reform in the melt state, a composite with a low melt-state viscosity is selected; to ensure that this behavior can occur at reasonable voltages, a composite with high conductivity is selected. Additionally, we choose a composite with a high brittleness to ensure that failure in the stiff-state occurred by brittle fracture instead of by necking. Although a number of composites tested meet these criteria, we select a low-molecular weight PCL filled with 20% carbon black for demonstration purposes.

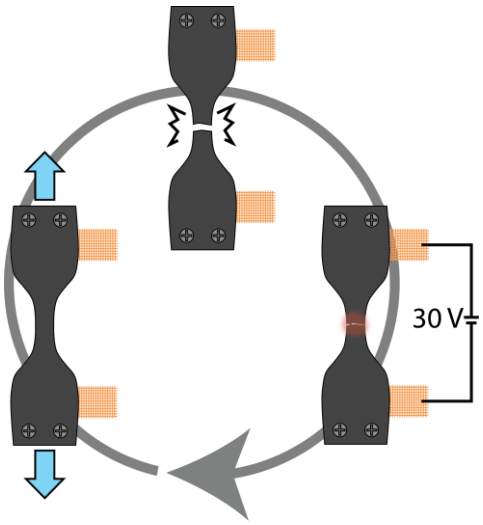

Figure 3.6: Electrically healable mechanical fuse cycle. **Top:** Fracture, **Right:** Electrically activated healing, **Left:** Repaired composite

3.4 Conclusions

This work shows how the composition of conductive thermoplastic materials can be tuned to create stiffness-switching devices for specific applications. Properties including melting point, conductivity, relaxation time, viscosity, switching ratio, and melt-state strain-at-break as a function of polymer molecular weight and filler loading fractions for two carbon fillers are studied. The properties critical to stiffness switching (e.g. conductivity, viscosity) are highly

interrelated (Figure 3.4); however, judicious selection of materials may help ameliorate the trade-off between favorable rheological properties and high conductivity shown in this work. Using this information, we inform the material selection for three stiffness switching applications, and show improved performance in both flexural and tensile stiffness switching, while demonstrating electrically activated healing. The findings from this work can be use to guide the further development of stiffness-switching devices for a variety of soft robotic and wearable applications.

4

Conclusion and Future Work

This work represents a comprehensive study of quasi-static stiffness switching using conductive thermoplastics. In Chapter 2, we demonstrated a novel through-thickness actuation strategy that reduces the required activation voltage and time, and enables the activation of arbitrary sheet geometries. In Chapter 3, we presented a deeper look into the composition of these composites, and the effects of composition on relevant stiffness-switching properties. Although this work provides a good basis for understanding and applying these materials, there are several areas ripe for future study, including the composite-electrode interface, alternative composite compositions, and the incorporation of these composites into robotic and wearable applications.

4.1 Improvements in the Composite-Electrode Interface

The reliability and stability of the cTP-electrode interface has been a persistent challenge for these materials. As these polymer composites transform between the solid state and the melt state, there arises an inevitable mismatch in mechanical impedance between the electrode and the stiffness-switching element, increasing the likelihood of failure at this interface. This may be addressed by emulating the techniques used to interface with liquid metal circuits (e.g. by stiffening the elastomeric casing at the interface), or by selecting stiffness-switching composites with characteristics that decrease this mismatch. For instance, certain carbon-PCL composites with high molecular weight and high loading fraction behave like pseudosolids or thermosets above the glass transition, which can improve the interface between a stiff electrode and the soft-

state composite. These properties, of course, limit the elasticity and deformability of devices using these materials; however, it may be possible to overcome these trade-offs by creating graded composites with different rheological and mechanical properties across their length.

Furthermore, the through-thickness electrode configuration demands that electrodes be both highly conductive and highly compliant, in order to deliver sufficient current to activate the composite and match its deformations in the soft state. Specifically, to ensure that heating occurs within the cTP composite, electrode resistance and the contact resistance between the electrode and the composite need to be significantly less than the resistance through the thickness of the composite, which can be as low as several ohms. In Chapter 2, we selected EGaIn as an electrode material because it possesses a low metallic resistance, fluidic deformability, and can be spray deposited on the composite surface to minimize the contact resistance. Although effective in actuating the composite, these electrodes proved unreliable with time, handling, and cycling, likely because of their susceptibility to smearing and oxidation.

With the lower composite resistances shown in Chapter 3, however, electrode materials with higher resistances but improved mechanical stability, such as conductive polymers[143,144], may become more feasible.

4.2 Investigations into the Composite Composition

Chapter 3 investigated the effects of filler material, filler loading fraction, and matrix molecular weight on the bulk properties of the stiffness-switching element. Over the course of these experiments, trade-offs between a number of characteristics, most notably electrical (i.e. conductivity) and rheological (i.e. viscosity, relaxation time, melt-state strain-at-break) properties arose. Although these relationships are based on the fundamental interactions between

rigid fillers and matrix materials, the materials selected for these studies do not necessarily optimize these properties. These tests cover a broad spectrum of common design dimensions for conductive composites, but represent only a small fraction of possible materials.

For instance, we investigated only two commonly available fillers: carbon black and carbon nanotubes. Conductive fillers and processing techniques have been extensively studied for use flexible, transparent, or lightweight electronics[145], and they should be similarly studied to help optimize the rheological and electrical properties for stiffness-switching applications. Furthermore, less traditional conductive fillers such as liquid metals or LMPA particles may help give highly conductive composites favorable rheological properties.

The matrix material is also an important area of future study. Other low-melting point polymers and polymer blends can be investigated, but even within the domain of PCL, there are a wide variety of chain modifications that can affect the mechanical, rheologial, and thermal properties of the composite. Preliminary tests with a PCL diol revealed that the melting point of PCL-based composites could be lowered by as much as 10 °C, while improving rheological characteristics (viscosity and relaxation time) and causing minimal changes to the conductivity (Appendix 5.3).

One problem that arose frequently over the course of these experiments, especially in the through-thickness activation mode presented in Chapter 2, was the appearance of hotspots in the stiffness-switching elements. After several activation-deactivation cycles, the heating that was initially spread evenly throughout the entire composite slowly became concentrated in one area. This localized heating was exacerbated over subsequent cycles until the majority of the composite failed to heat, while the hotspot temperature rose to dangerous levels. It is possible that this failure mode may be a result of uneven dispersion of conductive material throughout the

polymer matrix, since unequal current density can cause unequal heat generation within Joule heaters[91]. If this is the case, future work should focus on material combinations and manufacturing steps to ensure the homogeneity of the composite.

4.3 Development of Robotic and Wearable Applications

In Chapters 2 and 3, robotic and wearable demonstrations were developed as proofs-of-concept for the integration of conductive thermoplastic as a stiffness-switching element. Other work has demonstrated the utility of these composites in controlling soft robotic fingers and grippers[86,70], and tunable dry adhesion[87]. With the advances in actuation methodology and composition presented in this work, cTP-based stiffness-switching shows more potential than ever for use in soft robotic actuators.

Specifically, the low voltages and large surface area stiffness-switching afforded by the through-thickness actuation scheme developed in Chapter 2 can enable safe, reversible dry adhesion on a larger scale than that shown in Tatari et al.[87]. Subsurface stiffness has been shown to be a critical factor in determining the work of adhesion of two materials[100,83,146]; therefore, using thermoplastic stiffness-switching composites as a backing layer can enable effective switchable adhesion, especially when coupled with other structures, such as gecko-inspired microfibers[100,147,148].

Integration of these composites into robotic systems can be aided by the development of closed-loop temperature control. After melting, the cTP may experience thermal runaway as it receives a similar energy input although its specific heat is reduced. A thermocouple-based control system could improve the safety and response time of these systems, while minimizing the energy expenditure. A thermoelectric cooler could also be used to accelerate the cool-down

time and improve the bandwidth of the device.

With these refinements, these devices could be used to improve the load capacity of a soft gripper or be incorporated in a soft robot to decrease its energy consumption. For instance, a soft actuator can manipulate a gripper conform to a heavy object, while the stiffness switch can increase the gripper rigidity to prevent it from deforming when lifting the object. This concept has been demonstrated with many stiffness switches[67]; however, the stiffness-switching elements presented here could enable rapid, low-voltage manipulations. Similarly, a mobile, soft, hanging robot may be able to couple a stiffness-switching element with an actuator to achieve long-term passive hanging. These materials may be able to further augment the capabilities of robotic systems by leveraging the relationship between strain and resistance in conductive polymers to create a sensor that can switch between a microstrain gauge and a hyperelastic strech sensor.

Finally, the electrically activated healing modality shown in Chapter 3 has a strong potential for use in autonomous or mobile robotics. Soft robots may incorporate these devices as a component in an electrically healable mechanical fuse to prevent them from applying excessive force to an object, or as a way to heal damage to a stiff, internal skeleton. This feature may even be used to create one-way reconfigurable robot origami that can selectively fuse body segments.

5

Bibliography

[1] Carmel Majidi. Soft Robotics: A Perspective - Current Trends and Prospects for the Future. *Soft Robotics*, 1(1):5–11, 2014.

[2] Cecilia Laschi, Barbara Mazzolai, and Matteo Cianchetti. Soft robotics: Technologies and systems pushing the boundaries of robot abilities. *Science Robotics*, 1(1):eaah3690, 2016.

[3] Daniela Rus and Michael T Tolley. Design, fabrication and control of soft robots. *Nature*, 521(7553):467–475, 2015.

[4] Steven I. Rich, Robert J. Wood, and Carmel Majidi. Untethered soft robotics. *Nature Electronics*, 1(2):102–112, 2018.

[5] Mallory L. Hammock, Alex Chortos, Benjamin C K Tee, Jeffrey B H Tok, and Zhenan Bao. 25th anniversary article: The evolution of electronic skin (E-Skin): A brief history, design considerations, and recent progress. *Advanced Materials*, 25:5997–6038, 2013.

[6] Eric Markvicka, Steven Rich, Jiahe Liao, Hesham Zaini, Carmel Majidi, and I Background. Low-cost Wearable Human-Computer Interface with Conductive Fabric for STEAM Education. In *2018 IEEE Integrated STEM Education Conference (ISEC)*, pages 161–166, 2018.

[7] T. Yokota, P. Zalar, M. Kaltenbrunner, H. Jinno, N. Matsuhisa, H. Kitanosako, Y. Tachibana, W. Yukita, M. Koizumi, and T. Someya. Ultraflexible organic photonic skin. *Science Advances*, 2(4):e1501856–e1501856, 2016.

[8] Martin Weigel, Tong Lu, Gilles Bailly, Antti Oulasvirta, Carmel Majidi, and Jürgen Steimle.

iSkin. *Proceedings of the 33rd Annual ACM Conference on Human Factors in Computing Systems - CHI '15*, pages 2991–3000, 2015.

[9] C. Larson, B. Peele, S. Li, S. Robinson, M. Totaro, L. Beccai,

B. Mazzolai, and R. Shepherd. Highly stretchable electroluminescent skin for optical signaling and tactile sensing. *Science*,

351(6277):1071–1074, 2016.

[10] Yasutoshi Jimbo, Naoji Matsuhisa, Wonryung Lee, Peter Zalar, Hiroaki Jinno, Tomoyuki Yokota, Masaki Sekino, and Takao Someya. Ultraflexible Transparent Oxide/Metal/Oxide Stack Electrode with Low Sheet Resistance for Electrophysiological Measurements. *ACS Applied Materials and Interfaces*, 9(40):34744– 34750, 2017.

[11] Kyung In Jang, Kan Li, Ha Uk Chung, Sheng Xu, Han Na Jung, Yiyuan Yang, Jean Won Kwak, Han Hee Jung, Juwon Song, Ce Yang, Ao Wang, Zhuangjian Liu, Jong Yoon Lee, Bong Hoon Kim, Jae Hwan Kim, Jungyup Lee, Yongjoon Yu, Bum Jun Kim, Hokyung Jang, Ki Jun Yu, Jeonghyun Kim, Jung Woo Lee, Jae Woong Jeong, Young Min Song, Yonggang Huang, Yihui Zhang, and John A. Rogers. Self-assembled three dimensional network designs for soft electronics. *Nature Communications*, 8(May):15894, 2017.

[12] Yi Li and Minoru Hashimoto. PVC gel soft actuator-based wear- able assist wear for hip joint support during walking. *Smart Materials and Structures*, 26(12):0–12, 2017.

[13] Ciarán T. O'Neill, Nathan S. Phipps, Leonardo Cappello, Sabrina Paganoni, and Conor J. Walsh. A soft wearable robot for the shoulder: Design, characterization, and preliminary testing. *IEEE International Conference on Rehabilitation Robotics*, 02129:1672–1678, 2017.

[14] John a Rogers, Takao Someya, and Yonggang Huang. Materials and mechanics for stretchable

electronics. *Science*, 327:1603– 1607, 2010.

[15] Kadri Bugra Ozutemiz, James Wissman, Osman Burak Ozdoganlar, and Carmel Majidi. EGaIn-Metal Interfacing for Liquid Metal Circuitry and Microelectronics Integration. *Advanced Materials Interfaces*, 5(10):1–13, 2018.

[16] Jeonghyun Kim, Giovanni A. Salvatore, Hitoshi Araki, Antonio M. Chiarelli, Zhaoqian Xie, Anthony Banks, Xing Sheng, Yuhao Liu, Jung Woo Lee, Kyung In Jang, Seung Yun Heo, Kyoungyeon Cho, Hongying Luo, Benjamin Zimmerman, Joonhee Kim, Lingqing Yan, Xue Feng, Sheng Xu, Monica Fabiani, Gabriele Gratton, Yonggang Huang, Ungyu Paik, and John A. Rogers. Battery-free, stretchable optoelectronic systems for wireless optical characterization of the skin. *Science advances*, 2(8):e1600418, 2016.

[17] Yuji Gao, Hiroki Ota, Ethan W. Schaler, Kevin Chen, Allan Zhao, Wei Gao, Hossain M. Fahad, Yonggang Leng, Anzong Zheng, Furui Xiong, Chuchu Zhang, Li Chia Tai, Peida Zhao, Ronald S. Fearing, and Ali Javey. Wearable Microfluidic Diaphragm Pressure Sensor for Health and Tactile Touch Monitoring. *Advanced Materials*, 29(39):1701985, 2017.

[18] Matteo Cianchetti, Mariangela Manti, Vito Cacucciolo, and Cecilia Laschi. Stiffening in Soft Robotics: a review. *Robotics and Automation Magazine (under review)*, 23(3):93–106, 2016.

[19] Liyu Wang, Yang Yang, Yonghua Chen, Carmel Majidi, Fumiya Iida, Erin Askounis, and Qibing Pei. Controllable and reversible tuning of material rigidity for robot applications. *Materials Today*, 21(5):1–14, 2018.

[20] WILLIAM M. KIER and KATHLEEN K. SMITH. Tongues, tentacles and trunks: the biomechanics of movement in muscular hydrostats. *Zoological Journal of the Linnean Society*, 83(4):307–324, 1985.

[21] I.W. Hunter and S. Lafontaine. A comparison of muscle with artificial actuators.

[22] Tatsuo Motokawa. Connective Tissue Catch in Echinoderms. *Biological Reviews*, 59(2):255–270, 1984.

[23] Boyce S. Chang, Ravi Tutika, Joel Cutinho, Stephanie Oyola-Reynoso, Jiahao Chen, Michael D. Bartlett, and Martin M. Thuo. Mechanically triggered composite stiffness tuning through thermodynamic relaxation (ST3R). *Materials Horizons*, 5(3):416–422, 2018.

[24] Frank L Hammond III, Faye Wu, and H Harry Asada. Variable Stiffness Pneumatic Structures for Wearable Supernumerary Robotic Devices. In Antonio Bicchi and Wolfram Burgard, editors, *Robotics Research: Volume 1*, volume 1, pages 201–217. Springer International Publishing, 2018.

[25] Ali Shiva, Agostino Stilli, Yohan Noh, Angela Faragasso, Iris De Falco, Giada Gerboni, Matteo Cianchetti, Arianna Menciassi, Kaspar Althoefer, and Helge A. Wurdemann. Tendon-Based Stiffening for a Pneumatically Actuated Soft Manipulator. *IEEE Robotics and Automation Letters*, 1(2):632–637, 2016.

[26] Agostino Stilli, Helge A. Wurdemann, and Kaspar Althoefer. Shrinkable, stiffness-controllable soft manipulator based on a bio-inspired antagonistic actuation principle. In *IEEE International Conference on Intelligent Robots and Systems*, number 1, pages 2476–2481, 2014.

[27] Farahnaz Maghooa, Agostino Stilli, Yohan Noh, Kaspar Althoefer, and Helge A. Wurdemann. Tendon and pressure actuation for a bio-inspired manipulator based on an antagonistic principle. *Proceedings - IEEE International Conference on Robotics and Automation*, pages 2556–2561, 2015.

[28] Loai A.T. Al Abeach, Samia Nefti-Meziani, and Steve Davis. Design of a Variable Stiffness Soft

Dexterous Gripper. *Soft Robotics*, 00(00):soro.2016.0044, 2017.

[29] Koichi Suzumori, Shuichi Wakimoto, Kenta Miyoshi, and Kazuhiro Iwata. Long bending rubber mechanism combined contracting and extending fluidic actuators. *IEEE International Conference on Intelligent Robots and Systems*, pages 4454–4459, 2013.

[30] Tao Wang, Yue Li, Yuanjie Li, Jinhua Zhang, Jun Hong, and Michael Yu Wang. A Fluid-Filled Tubular Dielectric Elastomer Variable Stiffness Structure Inspired by the Hydrostatic Skeleton Principle *. In *IEEE International Conference on Robotics and Automation (ICRA)*, pages 1553–1558, 2018.

[31] Ying Shan, M. Philen, A. Lotfi, Suyi Li, C. E. Bakis, C. D. Rahn, and K.W. Wang. Variable Stiffness Structures Utilizing Fluidic Flexible Matrix Composites. *Journal of Intelligent Material Systems and Structures*, 20(4):443–456, 2008.

[32] Agostino Stilli, Luca Grattarola, Hauke Feldmann, Helge A Wurdemann, and Kaspar Althoefer. Variable Stiffness Links (VSL): Toward Inherently Safe Robotic Manipulators. *IEEE International conference on Robotics and Automation ICRA*, pages 4971– 4976, 2017.

[33] E. Brown, N. Rodenberg, J. Amend, a. Mozeika, E. Steltz, M. R. Zakin, H. Lipson, and H. M. Jaeger. From the Cover: Universal robotic gripper based on the jamming of granular material. *Proceedings of the National Academy of Sciences*, 107(44):18809–18814, 2010.

[34] Simon Hauser, Matthew Robertson, Auke Ijspeert, and Jamie Paik. JammJoint: A Variable Stiffness Device Based on Granular Jamming for Wearable Joint Support. *IEEE Robotics and Automation Letters*, 2(2):849–855, 2017.

[35] Andrew A. Stanley and Allison M. Okamura. Controllable Surface Haptics via Particle Jamming

and Pneumatics. *IEEE Transactions on Haptics*, 8(1):20–30, 2015.

[36] Ying Wei, Yonghua Chen, Yang Yang, and Yingtian Li. A soft robotic spine with tunable stiffness based on integrated ball joint and particle jamming. *Mechatronics*, 33:84–92, 2016.

[37] Sean Follmer, Daniel Leithinger, Alex Olwal, Nadia Cheng, and Hiroshi Ishii. Jamming User Interfaces: Programmable Particle Stiffness and Sensing for Malleable and Shape-Changing Devices. *Proceedings of the 25th annual ACM symposium on User interface software and technology - UIST '12*, pages 519–528, 2012.

[38] Nadia G. Cheng, Maxim B. Lobovsky, Steven J. Keating, Adam M. Setapen, Katy I. Gero, Anette E. Hosoi, and Karl D. Iagnemma. Design and analysis of a robust, low-cost, highly articulated manipulator enabled by jamming of granular media. *Proceedings - IEEE International Conference on Robotics and Automation*, pages 4328–4333, 2012.

[39] Matteo Cianchetti, Tommaso Ranzani, Giada Gerboni, Thrishantha Nanayakkara, Kaspar Althoefer, Prokar Dasgupta, and Arianna Menciassi. Soft Robotics Technologies to Address Shortcomings in Today's Minimally Invasive Surgery: The STIFF-FLOP Approach. *Soft Robotics*, 1(2):122–131, 2014.

[40] Iris De Falco, Matteo Cianchetti, and Arianna Menciassi. A soft multi-module manipulator with variable stiffness for minimally invasive surgery. *Bioinspiration and Biomimetics*, 12(5), 2017.

[41] Jifei Ou, Lining Yao, Daniel Tauber, Jürgen Steimle, Ryuma Niiyama, and Hiroshi Ishii. jamSheets. *Proceedings of the 8th International Conference on Tangible, Embedded and Embodied Interaction - TEI '14*, pages 65–72, 2013.

[42] Yashraj S. Narang, Alperen Degirmenci, Joost J. Vlassak, and Robert D. Howe. Transforming the Dynamic Response of Robotic Structures and Systems Through Laminar Jamming. *IEEE*

Robotics and Automation Letters, 3(2):688–695, 2018.

[43] A. Tonazzini, J. Shintake, C. Rognon, V. Ramachandran,S. Mintchev, and D. Floreano. Variable stiffness strip with strain sensing for wearable robotics. In *2018 IEEE International Conference on Soft Robotics, RoboSoft 2018*, number 1, pages 485–490. IEEE, 2018.

[44] Inrak Choi, Nick Corson, Lizzie Peiros, Elliot W. Hawkes, Sean Keller, and Sean Follmer. A Soft, Controllable, High Force Density Linear Brake Utilizing Layer Jamming. *IEEE Robotics and Automation Letters*, 3(1):450–457, 2018.

[45] Timothy M. Simon, Ross T. Smith, and Bruce H. Thomas. Wearable jamming mitten for virtual environment haptics. *Proceedings of the 2014 ACM International Symposium on Wearable Computers - ISWC '14*, pages 67–70, 2014.

[46] Yong Jae Kim, Shanbao Cheng, Sangbae Kim, and Karl Iagnemma. A novel layer jamming mechanism with tunable stiffness capability for minimally invasive surgery. *IEEE Transactions on Robotics*, 29(4):1031–1042, 2013.

[47] Stuart Diller, Carmel Majidi, and Steven H. Collins. A lightweight, low-power electroadhesive clutch and spring for exoskeleton actuation. *IEEE International Conference on Intelligent Robots and Systems*, 2016-June:682–689, 2016.

[48] Stuart B Diller, Steven H Collins, and Carmel Majidi. The effects of electroadhesive clutch design parameters on performance characteristics. *Journal of Intelligent Material Systems and Structures*, page 1045389X1879947, 2018.

[49] Vivek Ramachandran, Jun Shintake, and Dario Floreano. All-Fabric Wearable Electroadhesive Clutch. *Advanced Materials Technologies*, 1800313:1–14, 2018.

[50] Daniel M. Aukes, Barrett Heyneman, John Ulmen, Hannah Stuart, Mark R. Cutkosky, Susan Kim, Pablo Garcia, and Aaron Edsinger. Design and testing of a selectively compliant underactuated hand. *International Journal of Robotics Research*, 33(5):721– 735, 2014.

[51] Hiroya Imamura, Kevin Kadooka, and Minoru Taya. A variable stiffness dielectric elastomer actuator based on electrostatic chucking. *Soft Matter*, 13(18):3440–3448, 2017.

[52] Michael D. Bartlett, Navid Kazem, Matthew J. Powell-Palm, Xiaonan Huang, Wenhuan Sun, Jonathan A. Malen, and Carmel Majidi. High thermal conductivity in soft elastomers with elongated liquid metal inclusions. *Proceedings of the National Academy of Sciences*, 114(9):2143–2148, 2017.

[53] Hugo Rodrigue, Wei Wang, Dong Ryul Kim, and Sung Hoon Ahn. Curved shape memory alloy-based soft actuators and application to soft gripper. *Composite Structures*, 176:398–406, 2017.

[54] Hu Jin, Erbao Dong, Min Xu, Chunshan Liu, Gursel Alici, and Yang Jie. Soft and smart modular structures actuated by shape memory alloy (SMA) wires as tentacles of soft robots. *Smart Materials and Structures*, 25(8):085026, 2016.

[55] Toshiya Ishikawa and Taro Nakamura. Portability and antagonistic stiffness control for an shape memory alloy artificial muscle actuator protected by a rolled film tube. *IEEE/ASME International Conference on Advanced Intelligent Mechatronics, AIM*, 2016- Septe(2):220–227, 2016.

[56] A. Hadi, A. Yousefi-Koma, M. Elahinia, M. M. Moghaddam, and A. Ghazavi. A shape memory alloy spring-based actuator with stiffness and position controllability. *Proceedings of the Institution of Mechanical Engineers. Part I: Journal of Systems and Control Engineering*, 225(7):902–917, 2011.

[57] Toshiyuki Hino and Taka Maeno. Development of a Miniature Robot Finger with a Variable Stiffness Mechanism using Shape Memory Alloy. In *International Symposium on Robotics and Automation*, number 1, pages 1–8, 2004.

[58] Yanfei Cao, Feng Ju, Lei Zhang, Dongming Bai, Fei Qi, and Bai Chen. A novel variable-stiffness flexible manipulator actuated by shape memory alloy for minimally invasive surgery. In *Proceedings of the Institution of Mechanical Engineers, Part H: Journal of Engineering in Medicine*, number 29, page 095441191880292, 2018.

[59] Mojtaba Azadi, Saeed Behzadipour, and Garry Faulkner. Antagonistic variable stiffness elements. *Mechanism and Machine Theory*, 44(9):1746–1758, 2009.

[60] E. Rustighi, M. J. Brennan, and B. R. Mace. A shape memory alloy adaptive tuned vibration absorber: Design and implementation. *Smart Materials and Structures*, 14(1):19–28, 2005.

[61] Yeongjin Kim, Shing Shin Cheng, and Jaydev P. Desai. Active Stiffness Tuning of a Spring-Based Continuum Robot for MRI-Guided Neurosurgery. *IEEE Transactions on Robotics*, 34(1):1–11, 2018.

[62] Xuyang Ren, Guokai Zhang, Zufeng Shang, and Shuxin Wang. A Variable Stiffness Spring-Sponge Composite Tube with Fast Response and Shape Recovery. *Macromolecular Materials and Engineering*, 1800185:1800185, 2018.

[63] J. R. Capadona, K. Shanmuganathan, D. J. Tyler, S. J. Rowan, and C. Weder. Stimuli-Responsive Polymer Nanocomposites Inspired by the Sea Cucumber Dermis. *Science*, 319(5868):1370– 1374, 2008.

[64] Chen Qian, Taka-Aki ASOH, and Hiroshi Uyama. Sea Cucumber Mimicking Bacterial Cellulose Composite Hydrogel with Ionic Strength-sensitive Mechanical Adaptivity. *Chemical*

Communications, 2018.

[65] Kadhiravan Shanmuganathan, Jeffrey R. Capadona, Stuart J. Rowan, and Christoph Weder. Biomimetic mechanically adaptive nanocomposites. *Progress in Polymer Science*, 35(1-2):212–222, 2010.

[66] Fei Gao, Yinyu Zhang, Yongmao Li, Bing Xu, Zhiqiang Cao, and Wenguang Liu. Sea Cucumber-Inspired Autolytic Hydrogels Exhibiting Tunable High Mechanical Performances, Repairability, and Reusability. *ACS Applied Materials and Interfaces*, 8(14):8956– 8966, 2016.

[67] Jun Shintake, Bryan Schubert, Samuel Rosset, Herbert Shea, and Dario Floreano. Variable stiffness actuator for soft robotics using dielectric elastomer and low-melting-point alloy. *IEEE International Conference on Intelligent Robots and Systems*, 2015-Decem:1097–1102, 2015.

[68] Riku Takahashi, Tao Lin Sun, Yoshiyuki Saruwatari, Takayuki Kurokawa, Daniel R. King, and Jian Ping Gong. Creating Stiff, Tough, and Functional Hydrogel Composites with Low-Melting-Point Alloys. *Advanced Materials*, 30(16):1–7, 2018.

[69] Michelle C. Yuen, R. Adam Bilodeau, and Rebecca K. Kramer. Active Variable Stiffness Fibers for Multifunctional Robotic Fabrics. *IEEE Robotics and Automation Letters*, 1(2):708–715, 2016.

[70] Amir Mohammadi Nasab, Amin Sabzehzar, Milad Tatari, Carmel Majidi, and Wanliang Shan. A Soft Gripper with Rigidity Tunable Elastomer Strips as Ligaments. *Soft Robotics*, 4(4):soro.2016.0039, 2017.

[71] Trevor L. Buckner, Edward L. White, Michelle C. Yuen, R. Adam Bilodeau, and Rebecca K. Kramer. A move-and-hold pneumatic actuator enabled by self-softening variable stiffness materials. *IEEE International Conference on Intelligent Robots and Systems*, 2017:3728–3733,

2017.

[72] Thomas P. Chenal, Jennifer C. Case, Jamie Paik, and Rebecca K. Kramer. Variable stiffness fabrics with embedded shape memory materials for wearable applications. In *IEEE International Conference on Intelligent Systems*: pages 2827-2831, 2014.

[73] Alice Tonazzini, Stefano Mintchev, Bryan Schubert, Barbara Mazzolai, Jun Shintake, and Dario Floreano. Variable Stiffness Fiber with Self-Healing Capability. *Advanced Materials*, pages 10142–10148, 2016.

[74] Wanliang Shan, Tong Lu, and Carmel Majidi. Soft-matter composites with electrically tunable elastic rigidity. *Smart Materials and Structures*, 22(8):085005, 2013.

[75] L Zheng, S Yoshida, Y Morimoto, H Onoe, and S Takeuchi. Pneumatic Balloon Actuator With Tunable Bending Points. *28th IEEE International Conference on Micro Electro Mechanical Systems (MEMS)*, pages 18–21, 2015.

[76] Ilse M. Van Meerbeek, Benjamin C. Mac Murray, Jae Woo Kim, Sanlin S. Robinson, Perry X. Zou, Meredith N. Silberstein, and Robert F. Shepherd. Morphing Metal and Elastomer Bicontinuous Foams for Reversible Stiffness, Shape Memory, and Self-Healing Soft Machines. *Advanced Materials*, 28:2801–2806, 2016.

[77] Bryan E. Schubert and Dario Floreano. Variable stiffness material based on rigid low-melting-point-alloy microstructures embedded in soft poly(dimethylsiloxane) (PDMS). *RSC Advances*, 3(46):24671, 2013.

[78] Nathan Lazarus, Sarah S. Bedair, and Christopher Meyer. Remoldable inductors based on self-heating fusible alloys. *Proceedings of IEEE Sensors*, 2014-Decem(December):1551–1554, 2014.

[79] H A O Yufei, Wang Tianmiao, Fang Xi, Yang Kang, M A O Ling, Guan Juan, and W E N Li. A

Variable Stiffness Soft Robotic Gripper with Low-Melting-Point Alloy. In *Proceedings of the 36th Chinese Control Conference*, pages 6781–6786, 2017.

[80] Yufei Hao, Tianmiao Wang, Zhexin Xie, Wenguang Sun, Zemin Liu, Xi Fang, Minxuan Yang, and Li Wen. A eutectic-alloy-infused soft actuator with sensing, tunable degrees of freedom, and stiffness properties. *Journal of Micromechanics and Microengineering*, 28(2), 2018.

[81] Christophe Chautems, Alice Tonazzini, Dario Floreano, and Bradley J. Nelson. A variable stiffness catheter controlled with an external magnetic field. *IEEE International Conference on Intelligent Robots and Systems*, 2017-Septe:181–186, 2017.

[82] Wei Wang, Hugo Rodrigue, and Sung Hoon Ahn. Smart soft composite actuator with shape retention capability using embedded fusible alloy structures. *Composites Part B: Engineering*, 78:507–514, 2015.

[83] Zhou Ye, Guo Zhan Lum, Sukho Song, Steven Rich, and Metin Sitti. Gallium Adhesion: Phase Change of Gallium Enables Highly Reversible and Switchable Adhesion (Adv. Mater. 25/2016). *Advanced Materials*, page 5087, 2016.

[84] Majid Taghavi, Tim Helps, Boxiong Huang, and Jonathan Rossiter. 3D-Printed Ready-To-Use Variable-Stiffness Structures. *IEEE Robotics and Automation Letters*, 3(3):1–1, 2018.

[85] Steven Rich, Sung-Hwan Jang, Yong-Lae Park, and Carmel Majidi. Liquid Metal-Conductive Thermoplastic Elastomer Integration for Low-Voltage Stiffness Tuning. *Advanced Materials Technologies*, 1700179:1700179, 2017.

[86] Wanliang Shan, Stuart Diller, Abbas Tutcuoglu, and Carmel Majidi. Rigidity-tuning conductive elastomer. *Smart Materials and Structures*, 24(6):065001, 2015.

[87] Milad Tatari, Amir Mohammadi Nasab, Kevin T. Turner, and Wanliang Shan. Dynamically

Tunable Dry Adhesion via Subsurface Stiffness Modulation. *Advanced Materials Interfaces*, 1800321:1–7, 2018.

[88] M Andy McEvoy and Nikolaus Correll. Thermoplastic variable stiffness composites with embedded, networked sensing, actuation, and control. *Journal of Composite Materials*, 49(15):1799–1808, 2015.

[89] Huu Minh Le, Thanh Nho Do, Lin Cao, and Soo Jay Phee. Towards active variable stiffness manipulators for surgical robots. *Proceedings - IEEE International Conference on Robotics and Automation*, pages 1766–1771, 2017.

[90] Hua Dong and Glenn M Walker. Adjustable stiffness tubes via thermal modulation of a low melting point polymer. *Smart Materials and Structures*, 21(4):042001, 2012.

[91] Abbas Tutcuoglu, Carmel Majidi, and Wanliang Shan. Nonlinear thermal parameter estimation for embedded internal Joule heaters. *International Journal of Heat and Mass Transfer*, 97:412–421, 2016.

[92] Michele Folgheraiter, Bauyrzhan Aubakir, and Huseyin Atakan Varol. Thermally-Controlled Coiled Polymeric Wire as a Novel Variable Elastic Element. *IEEE/ASME International Conference on Advanced Intelligent Mechatronics, AIM*, pages 466–471, 2017.

[93] G. Mcknight, R. Doty, A. Keefe, G. Herrera, and C. Henry. Segmented Reinforcement Variable Stiffness Materials for Reconfigurable Surfaces. *Journal of Intelligent Material Systems and Structures*, 21(17):1783–1793, 2010.

[94] Yu Qiu, Zhi Ren, Wei Hu, Chao Liu, and Qibing Pei. Bistable electroactive polymer with sharp rigid-to-rubbery phase transition. In *Electroactive Polymer Actuators and Devices (EAPAD) 2016*, volume 9798, page 97981U, 2016.

[95] Yang Yang, Yonghua Chen, Yingtian Li, Zheng Wang, and Yunquan Li. Novel Variable-

Stiffness Robotic Fingers with Built-In Position Feedback. *Soft Robotics*, 00(00):soro.2016.0060, 2017.

[96] Wei Wang and Sung-Hoon Ahn. Shape Memory Alloy-Based Soft Gripper with Variable Stiffness for Compliant and Effective Grasping. *Soft Robotics*, 4(4):soro.2016.0081, 2017.

[97] Amir Firouzeh, Marco Salerno, and Jamie Paik. Stiffness Control with Shape Memory Polymer in Underactuated Robotic Origamis. *IEEE Transactions on Robotics*, 33(4):765–777, 2017.

[98] Aditya Balasubramanian, Mike Standish, and Christopher J. Bettinger. Microfluidic thermally activated materials for rapid control of macroscopic compliance. *Advanced Functional Materials*, 24(30):4860–4866, 2014.

[99] Kazuto Takashima, Jonathan Rossiter, and Toshiharu Mukai. McKibben artificial muscle using shape-memory polymer. *Sensors and Actuators, A: Physical*, 164(1-2):116–124, 2010.

[100] Seok Kim, Metin Sitti, Tao Xie, and Xingcheng Xiao. Reversible dry micro-fibrillar adhesives with thermally controllable adhesion. *Soft Matter*, 5(19):3689, 2009.

[101] Yang Yang, Yonghua Chen, Yingtian Li, Z.Q. Chen, Michael, and Ying Wei. Bioinspired Robotic Fingers Based on Pneumatic Actuator and 3D Printing of Smart Material. *Soft Robotics*, 4(2):soro.2016.0034, 2017.

[102] R. C. Laible. *Ballistic Materials and Penetration Mechanics*. Elsevier, 1982.

[103] Galal Zaki Said. Orthopaedics in the dawn of civilisation, practices in ancient Egypt. *International Orthopaedics*, 38(4):905–909, 2014.

[104] Valerie Steele. *The corset: A cultural history*. Yale University Press, 2003.

[105] Lawrence Barfield. The iceman reviewed. *Antiquity*, 68(258):10– 26, 1994.

[106] Jianyou Li and Hiroya Tanaka. Rapid customization system for 3D-printed splint using programmable modeling technique - a practical approach. *3D Printing in Medicine*, 4(5), 2018.

[107] Gregory S. Aldrete, Scott M. Bartell, and Alicia Aldrete. *Reconstruction ancient linen body armor: Unraveling the linothorax mystery*. JHU Press, 2013.

[108] Hu Liu, Yilong Li, Kun Dai, Guoqiang Zheng, Chuntai Liu, Changyu Shen, Xingru Yan, Jiang Guo, and Zhanhu Guo. Electrically conductive thermoplastic elastomer nanocomposites at ultralow graphene loading levels for strain sensor applications. *Journal of Materials Chemistry C*, 4(1):157–166, 2015.

[109] Patrick F. Flowers, Christopher Reyes, Shengrong Ye, Myung Jun Kim, and Benjamin J. Wiley. 3D printing electronic components and circuits with conductive thermoplastic filament. *Additive Manufacturing*, 18:156–163, 2017.

[110] Robert Shanks and Ing Kong. *Thermoplastic elastomers*. InTech, Rijeka, Croatia, 2012.

[111] Maris Knite, Valdis Teteris, Aleksandra Kiploka, and Jevgenijis Kaupuzs. Polyisoprene-carbon black nanocomposites as tensile strain and pressure sensor materials. *Sensors and Actuators, A: Physical*, 110(1-3):142–149, 2004.

[112] Seow Jecg Chin, Sesha Vempati, Paul Dawson, Maris Knite, Artis Linarts, Kaspars Ozols, and Tony McNally. Electrical conduction and rheological behaviour of composites of poly(ε-caprolactone) and MWCNTs. *Polymer*, 58:209–221, 2015.

[113] J C Landsman, W H Seitz, A I Froimson, R B Leb, and E J Bachner. Splint immobilization of gamekeeper's thumb. *Orthopedics*, 18(12):1161–5, 1995.

[114] Timothy John Baumgartner, Daniel Robert; Baumgartner. Low-temperature reusable thermoplastic splint, 2009.

[115] Waseem Khan, Rahul Sharma, and Parveen Saini. *Carbon Nanotube-Based Polymer Composites: Synthesis, Properties and Applications*. InTech, 2017.

[116] Kesong Hu, Dhaval D. Kulkarni, Ikjun Choi, and Vladimir V. Tsukruk. Graphene-polymer nanocomposites for structural and functional applications. *Progress in Polymer Science*, 39(11):1934– 1972, 2014.

[117] Wolfgang Bauhofer and Josef Z. Kovacs. A review and analysis of electrical percolation in carbon nanotube polymer composites. *Composites Science and Technology*, 69(10):1486–1498, 2009.

[118] Alfredo Bello, Estrella Laredo, Jesús R. Marval, Mario Grimau, María L. Arnal, Alejandro J. Müller, Benoit Ruelle, and Philippe Dubois. Universality and percolation in biodegradable poly(ε-caprolactone)/multiwalled carbon nanotube nanocomposites from broad band alternating and direct current conductivity at various temperatures. *Macromolecules*, 44(8):2819–2828, 2011.

[119] Arun K. Kota, Bani H. Cipriano, Matthew K. Duester berg, Alan L. Gershon, Dan Powell, Srinivasa R. Raghavan, and Hugh A. Bruck. Electrical and rheological percolation in polystyrene/MWCNT nanocomposites. *Macromolecules*, 40(20):7400–7406, 2007.

[120] L. Li, W. H. Ruan, M. Q. Zhang, and M. Z. Rong. Studies on the selective localization of multi-walled carbon nanotubes in blends of poly(vinylidene fluoride) and polycaprolactone. *Express Polymer Letters*, 9(1):77–83, 2015.

[121] Jizhao Liang and Quanquan Yang. Aggregate structure and percolation behavior in polymer/carbon black conductive composites. *Journal of Applied Physics*, 102(8), 2007.

[122] Cynthia A. Mitchell and Ramanan Krishnamoorti. Dispersion of single-walled carbon nanotubes

in poly(ε-caprolactone). *Macromolecules*, 40(5):1538–1545, 2007.

[123] Christian Penu, Guo-Hua Hu, Amaia Fernandez, Philippe Marchal, and Lionel Choplin. Rheological and Electrical Percolation Thresholds of Carbon Nanotube/Polymer Nanocomposites. *Polymer Engineering and Science*, 2012.

[124] Kai Zhang, Gen Hui Li, La Mei Feng, Ning Wang, Jiang Guo, Kai Sun, Kai Xin Yu, Jian Bing Zeng, Tingxi Li, Zhanhu Guo, and Ming Wang. Ultralow percolation threshold and enhanced electromagnetic interference shielding in poly(l-lactide)/multiwalled carbon nanotube nanocomposites with electrically conductive segregated networks. *Journal of Materials Chemistry C*, 5(36):9359–9369, 2017.

[125] Ming Wen, Xiaojie Sun, Lin Su, Jiabin Shen, Jiang Li, and Shaoyun Guo. The electrical conductivity of carbon nanotube/carbon black/polypropylene composites prepared through multistage stretching extrusion. *Polymer*, 53(7):1602– 1610, 2012.

[126] Fangming Du, Robert C. Scogna, Wei Zhou, Stijn Brand, John E. Fischer, and Karen I. Winey. Nanotube networks in polymer nanocomposites: Rheology and electrical conductivity. *Macromolecules*, 37(24):9048–9055, 2004.

[127] Xiaoming Xu, Chuanhua Gao, Qiang Zheng, and Xian Jiang. Linear/Nonlinear Rheological Properties and Percolation Threshold of Polydimethylsiloxane Filled with Calcium Carbonate. *Journal of the Society of Rheology, Japan*, 35(5):283–291, 2007.

[128] Tony McNally, Petra Pötschke, Peter Halley, Michael Murphy, Darren Martin, Steven E.J. Bell, Gerard P. Brennan, Daniel Bein, Patrick Lemoine, and John Paul Quinn. Polyethylene multiwalled carbon nanotube composites. *Polymer*, 46(19 SPEC. ISS.):8222–8232, 2005.

[129] Nazbanoo Noroozi. *Rheology And Processing Of Biodegradable Poly(e-caprolactone)*

Polyesters And Their Blends With Polylactides. PhD thesis, University of British Columbia, 2013.

[130] Yogesh M. Joshi and Morton M. Denn. Rupture of entangled polymeric liquids in elongational flow with dissipation. *Journal of Rheology*, 48(3):591, 2004.

[131] A. Ya. Malkin and C. J. S. Petrie. Some conditions for rupture of polymer liquids in extension. *Journal of Rheology*, 41(1):1–25, 1997.

[132] Zdeneˇk Starý, Magdalena Papp, and Teodor Burghelea. Deformation regimes, failure and rupture of a low density polyethylene (LDPE) melt undergoing uniaxial extension. *Journal of Non-Newtonian Fluid Mechanics*, 219:35–49, 2015.

[133] Jiji Abraham, T Sharika, Soney C George, and Sabu Thomas. Rheological Percolation in Thermoplastic Polymer Nanocomposites. *Rheology: Open access*, 1(1):1–15, 2017.

[134] Jan Sumfleth, Samuel T. Buschhorn, and Karl Schulte. Comparison of rheological and electrical percolation phenomena in carbon black and carbon nanotube filled epoxy polymers. *Journal of Materials Science*, 46(3):659–669, 2011.

[135] Yu S. Lipatov, V. F. Babich, and V. F. Rosovizky. Effect of filler on the relaxation time spectra of filled polymers. *Journal of Applied Polymer Science*, 20(7):1787–1794, 1976.

[136] Yihu Song and Qiang Zheng. Linear rheology of nanofilled polymers. *Journal of Rheology*, 59(1):155–191, 2015.

[137] Ji Zhao Liang, De Rong Duan, Chak Yin Tang, Chi Pong Tsui, Da Zhu Chen, and Shui Dong Zhang. Tensile properties of polycaprolactone/nano-CaCO3 composites. *Journal of Polymer Engineering*, 34(1):69–73, 2014.

[138] Ji Zhao Liang, Lin Zhou, Chak Yin Tang, and Chi Pong Tsui. Crystallization properties of polycaprolactone composites filled with nanometer calcium carbonate. *Journal of Applied Polymer Science*, 128(5):2940–2944, 2013.

[139] Bernardo Marinho, Marcos Ghislandi, Evgeniy Tkalya, Cor E. Koning, and Gijsbertus de With. Electrical conductivity of compacts of graphene, multi-wall carbon nanotubes, carbon black, and graphite powder. *Powder Technology*, 221:351–358, 2012.

[140] Michael Rubinstein and Ralph H. Colby. Polymer physics, 2003.

[141] R. Adam Bilodeau and Rebecca K. Kramer. Self-Healing and Damage Resilience for Soft Robotics: A Review. *Frontiers in Robotics and AI*, 4(October), 2017.

[142] Hongsheng Luo, Xingdong Zhou, Yuncheng Xu, Huaquan Wang, Yongtao Yao, Guobin Yi, and Zhifeng Hao. Multi-stimuli triggered self-healing of the conductive shape memory polymer composites. *Pigment and Resin Technology*, 47(1):1–6, 2018.

[143] Andrew Fassler and Carmel Majidi. Liquid-Phase Metal Inclusions for a Conductive Polymer Composite. *Advanced Materials*, 27(11):1928–1932, 2015.

[144] Naoji Matsuhisa, Daishi Inoue, Peter Zalar, Hanbit Jin, Yorishige Matsuba, Akira Itoh, Tomoyuki Yokota, Daisuke Hashizume, and Takao Someya. Printable elastic conductors by in situ formation of silver nanoparticles from silver flakes. *Nature Materials*, 16(8):834–840, 2017.

[145] Samira Naghdi, Kyong Yop Rhee, David Hui, and Soo Jin Park. A Review of Conductive Metal Nanomaterials as Conductive, Transparent, and Flexible Coatings, Thin Films, and Conductive Fillers: Different Deposition Methods and Applications. *Coatings*, 8(8):278, 2018.

[146] Michael D Bartlett and Alfred J Crosby. Scaling normal adhesion force capacity with a

generalized parameter. *Langmuir : the ACS journal of surfaces and colloids*, 29(35):11022–7, sep 2013.

[147] Metin Sitti and Ronald S. Fearing. Synthetic gecko foot-hair micro/nano-structures as dry adhesives. *Journal of Adhesion Science and Technology*, 17(8):1055–1073, jan 2003.

[148] Yiğit Mengüç, Sang Yoon Yang, Seok Kim, John A. Rogers, and Metin Sitti. Gecko-Inspired Controllable Adhesive Structures Applied to Micromanipulation. *Advanced Functional Materials*, 22(6):1246–1254, mar 2012.

6

Appendix

6.1 Characterization of Conductive Thermoplastic Stiffness-Switching Composites: Fabrication and Experiments

Thermal Characterization The melting and crystallization points were found using a differential scanning calorimeter (DSC Q20, TA Instruments). Three cycles were performed between 0 °C and 80 °C at a rate of 10.0 °C min^{-1}. The maxima and minima of cycles 2 and 3 were averaged to calculate the melting point and crystallization.

Modulus Measurements The stiff and soft moduli were tested using a universal materials testing machine (Model 5969, Instron). A 2.2 mm hole was cut in 1 cm × 5 cm strips of carbon-PCL, and they were embedded in a 5.5 mm layer of silicone rubber (Ecoflex 00-30, Smooth On). This layer prevented the carbon-PCL from flowing while in the melt state, allowing the overall stiffness of the carbon-PCL-silicone switch to be measured. A screw was placed through the hole in the strip and the holes in two acrylic plates, which were attached to the grips of the universal materials testing machine. A 1-1.5% strain was applied at a rate of 0.25 mm s^{-1}. The stiff-state modulus was found by taking the average fit of the stress-strain curve over two cycles, after ignoring the initial cycle. Three different samples were used for each data point. To find the soft-state modulus, a toaster oven (Mainstays) was modified to fit over the universal materials testing machine, and the temperature was set to 5 °C above the melting point of PCL, as determined by DSC, measured with a thermocouple embedded in the sample (K-Type, Traceable). Silicone

rubber adhesive (Sil-Poxy, Smooth-On) was applied to the silicone rubber and the carbon-PCL for the soft-state modulus tests to prevent tearing at the holes. The same procedure used for the stiff-state modulus tests was conducted within this heating chamber.

Conductivity Measurements To test the bulk conductivity of these sheets, 1 cm × 5 cm strips were measured using calipers and connected to a 4-point ohmmeter (34401A, Agilent). Three sheets were fabricated at each composition, from which 9 resistance measurements were taken each.

Rheological Measurements Crossover relaxation time and dynamic viscosity were measured using a rheometer (Gemini 200, Bohlin) with a parallel plate geometry (2.5 cm diameter) and a gap size of 1000 µm. The samples were compressed to achieve the desired thickness, which may have caused the filler to align, causing minor changes to the rheological properties measured [123]. The temperature was set to 5 °C above the melting temperature, as determined by DSC. Frequency sweep tests using a strain of 0.01 were conducted on samples cut from three different sheets. The relaxation time was found by taking the inverse of the

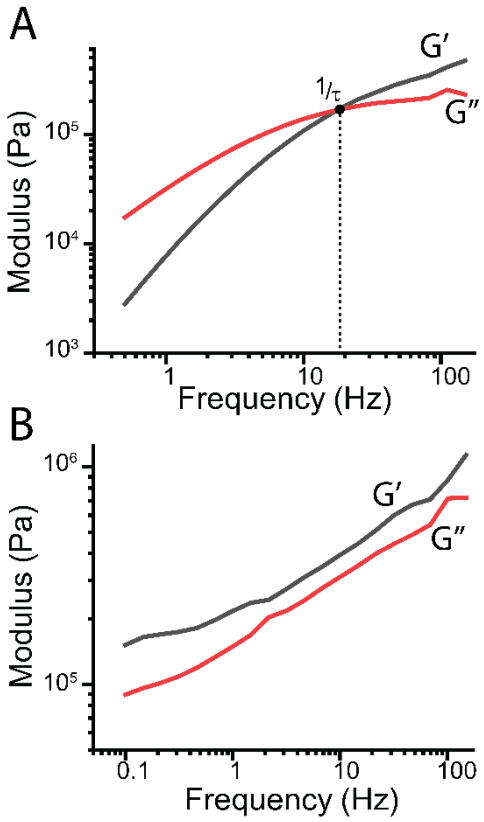

Figure 5.1: (A) An example of a *G'-G"* plot of a composite (pure intermediate-molecular weight PCL) below the percolation threshold (B) An example *G'-G"* plot of a composite (15% CB loading in low-molecular weight PCL) above the percolation threshold.

frequency where the storage modulus *G'* crossed below the loss modulus, *G"* (Figure 5.1 A). For samples where this crossover occurred at a frequency above the limits of the rheometer, the crossover frequency was found by interpolation. When *G'* and *G"* ran parallel without crossing over, the composite was considered to be above the rheological percolation threshold, with $\tau \rightarrow \infty$ [133] (Figure 5.1 B). The viscosity was evaluated at 1 Hz.

Melt Fracture Tests Melt fracture tests were conducted within the same universal materials testing machine and heating chamber used during the soft-state modulus tests, with the temperature set to 5 °C above the melting point, measured with a thermocouple (K-Type, Traceable). The samples, which were identical to those used in the modulus tests, were stretched in front of a camera up to 150% strain at a rate of 0.5 mm s^{-1}. The point at which tearing initiated in the carbon-PCL was visually determined from the video. Samples that survived past 150% strain were said to experience no melt fracture. Three different samples were used for each data point.

6.2 Development of Stiffness-Switching Demonstrations

Tensile Stiffness-Switching Tendon A sheet of cTP (20% carbon black filler embedded in a low-molecular weight PCL) was cut into a rectangular strip using a 30 W CO_2 laser cutter (VLS 3.50, Universal Laser Systems). The samples were softened in a 100 °C oven for 5 min, and leads made from copper mesh (22 per in., 0.015 in. wire diameter, TWP Inc.) were pressed into the thermoplastic by hand. The samples were then embedded in a 5.5 mm layer of silicone rubber (Ecoflex 00-30, Smooth-On): a 1.5 mm sheet of silicone rubber was cured and laid on the bottom of a 3D-printed mold (Objet 24, Stratsys). The cTP strip was laid on top of this sheet, and

uncured silicone rubber was poured over top, ensuring that a small amount of copper protruded from the rubber. The devices were cured in the oven at 60 °C for 1 h.

The stiffness switch was connected to a power supply (KPS3010D, Eventek) and 30 V was applied, causing the switch to heat up. When the surface temperature was measured to be 60 °C by an IR camera (C2, FLIR), the switch was disconnected and repeatedly stretched by hand. After several cycles, the switch was placed on the table and allowed to restiffen.

Flexural Stiffness-Switching Strip A sheet of cTP (15% carbon black filler embedded in an intermediate-molecular weight PCL) was cut into a long strip (20 cm × 1 cm) using a 30 W CO_2 laser cutter (VLS 3.50, Universal Laser Systems). The strip was placed in an acrylic mold, sandwiched between two sheets of copper mesh (200 per in., 0.002 in wire diameter, TWP Inc.), and compressed at 75 °C in a heat press. After the cTP had cooled, and the excess copper mesh was removed, the strip was embedded in a 5.5 mm layer of silicone rubber (Ecoflex 00-30, Smooth-On): a 1.5 mm sheet of silicone rubber was cured and laid on the bottom of a 3D-printed mold (Objet 24, Stratsys). The cTP strip was laid on top of this sheet, and uncured silicone rubber was poured over top, ensuring that a small amount of copper protruded from the rubber. The devices were cured in the oven at 60 °C for 30 min.

The stiffness switch was connected to a power supply (KPS3010D, Eventek), and 5 V–10 V was applied until the surface temperature was measured to be 60 °C by an IR camera (C2, FLIR). The switch was disconnected from the voltage source, and wrapped around a participant's wrist, where it was allowed to cool. After it had restiffened, the switch was reconnected to the power supply, and 5 V–10 V was applied until the surface temperature was measured to be 60 °C by an IR camera (C2, FLIR). The switch was disconnected from the voltage source and unwrapped

from the participants wrist. It was flattened on the countertop and allowed to restiffen.

Electrically Healable Mechanical Fuse A sheet of cTP (20% carbon black filler embedded in a low-molecular weigth PCL) was cut into a dogbone shape using a 30 W CO_2 laser cutter (VLS 3.50, Universal Laser Systems). The narrow section of the dogbone was 3.25 mm, while the ends were 14 mm, large enough to accommodate two screws for attaching to the clamps of a universal materials testing machine (Model 5969, Instron). The samples were softened in a 100 °C oven for 5 min, and leads made from copper mesh (22 per in., 0.015 in. wire diameter, TWP Inc.) were pressed into the thermoplastic by hand below the screws. The samples were then embedded in a 5.5 mm layer of silicone rubber (Ecoflex 00-30, Smooth-On): a 1.5 mm sheet of silicone rubber was cured and laid on the bottom of a 3D-printed mold (Objet 24, Stratsys). The dogbone sample was laid on top of this sheet, and uncured silicone rubber was poured over top, ensuring that a small amount of copper protruded from the rubber. The samples were cured in the oven at 60 °C for 1 h.

An extension rate of 0.5 mm s^{-1} was applied to the dogbone sample until fracture occurred. In the video, these samples were broken by hand. The sample was returned to its previous length and a voltage of 30 V was applied at the ends. The length of the sample was decreased by about 1 mm until current began to flow. After the temperature of the composite reached 60 °C, as measured by an IR camera (C2, FLIR), the current was extinguished. After the dogbone was allowed to cool, the tensile test was conducted again.

A maximum of 52.7 N was measured before the first fracture. After the sample was healed, a maximum force of 34.2 N was measured, yielding a recovery strength of 65%.

6.3 Preliminary Studies of Chain-Modified PCL

Initial tests showing the behavior of chain-modified PCL (CAPA 8502A: $M_w \approx 50\ 000$ g mol−1, a co-polyester PCL diol) were conducted. These tests are incomplete and should be expanded in future work. Both the melting point T_m and crystallization point T_c of PCL-diol composites were significantly reduced, which could allow for stiffness switches with shorter activation times, longer deactivation times, and reduced energy input (Figure 5.2 A). There is little difference between PCL composites, and PCL-diol composites of similar molecular weight (Figure 5.2). Finally, although the viscosity of these diol composites is on the order of the high-molecular weight PCL composites, preliminary relaxation time data indicates that these composites may remain below percolation for higher loading fractions than other PCL formulations tested (Figure 5.2C-D). Together, these studies show that these chain modifications may help to create devices with excellent rheological properties that do not sacrifice electrical conductivity.

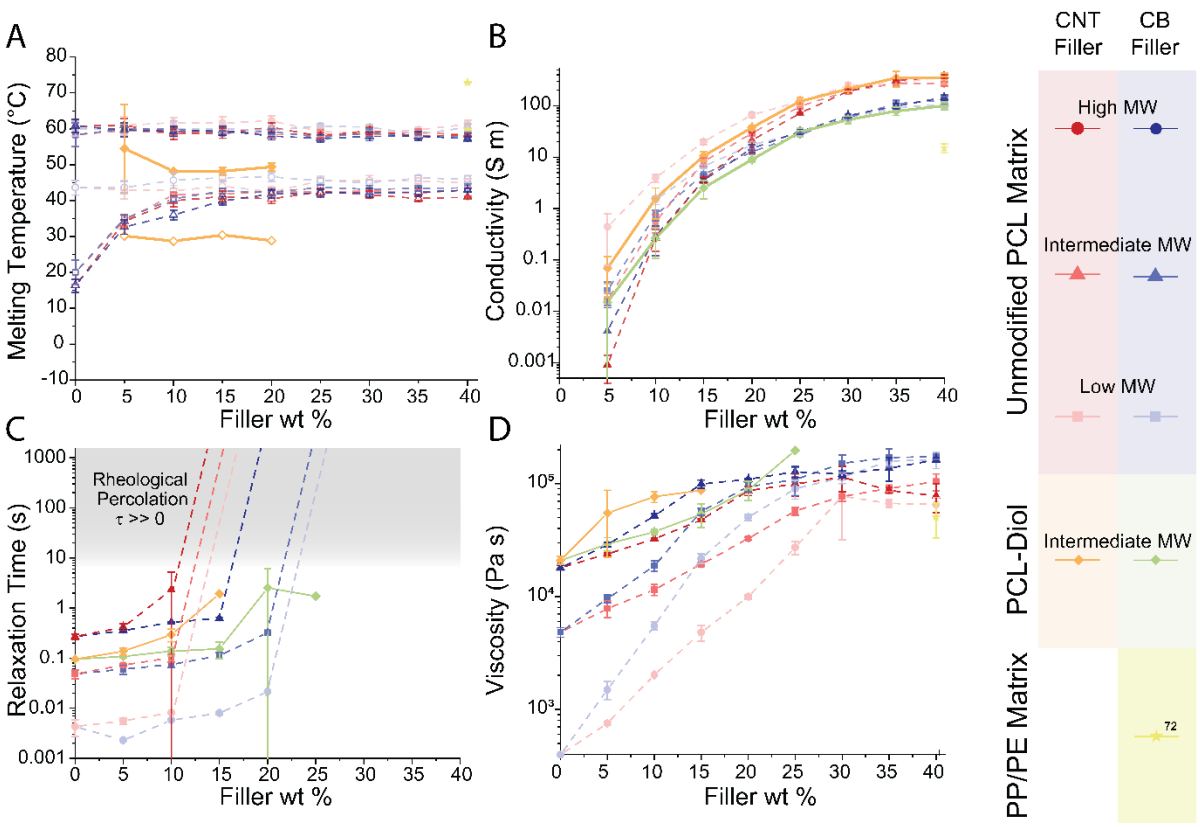

Figure 5.2: Preliminary data for standard PCL and PCL diol matrix material (A) The relationship between melting point T_m (filled symbols) and crystallization point T_c (open symbols) and filler loading fraction. (B) The relationship between conductivity and filler loading fraction. (C) The relationship between relaxation time τ and filler loading fraction. (D) The relationship between dynamic viscosity and filler loading fraction.